Chapter - 4

Theoretical Analysis for Radiators Performance

This chapter contains three sections. In first section the energetic and exergetic theoretical performance analyses of wavy fin, louvered fin and rectangular fin flat tube automotive radiator with various base fluids, nanofluids and hybrid nanofluids as radiator coolant have been discussed. The second section contains the theoretical performance of radiator with different fin materials and the third section deals with the theoretical performance analysis with different configuration and orientations of radiators.

4.1 Performance analysis on the basis of various coolants

The searching of an alternative heat transfer fluid for overall performance improvement to enhance the cooling rate is not ending. Water and water mixed with anti-freezing agents such as such as EG and PG are the traditional coolants for automotive radiator. Recently nanofluid have been proposed as coolant for automotive radiator, but the operation and long term stability are major challenges for nanofluid and hybrid nanofluids. In this respect, sugar cane juice, which has very similar freezing and boiling points with water, and a new coolant optimum PG brine (25% PG brine), may be an alternative coolants and also use of wavy, louvered and rectangular fin with flat tube are the effective ways to improve the radiator performance.

4.1.1 Mathematical Modelling

The mathematical model has been developed based on first law of thermodynamics including heat transfer and fluid flow effects. The following assumptions have been made for the theoretical analysis:

(i) Steady state heat transfer and fluid flow.

(ii) Both air flow and coolant flow are uniform.

(iii) All the heat rejected from coolant, absorbed by air flow through radiator.

(iv) Properties of coolants and air have been taken based on mean temperature.

(a) Wavy fin radiator

The wavy finned automotive radiator considered in this study is shown in Fig. 4.1, which consists of 64 vertical flat coolant tubes made of brass and 346 continuous wavy fins made of aluminum alloy. The geometrical parameters are described in the Table 4.1.

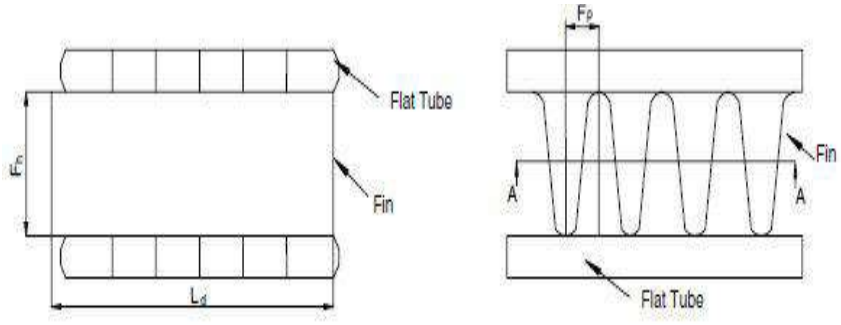

Fig. 4.1: Geometric parameters for wavy fin radiator [50]

Table 4.1: Surface core geometry of tubes and fins (Wavy fin radiator)

Description	Air side	Coolant side
Fin pitch	4.46fins/cm	
Core Width, W_c	382 mm	
Core height, H_c	491 mm	
Core depth, F_d	44 mm	
Fin metal thickness	1 mm	
Hydraulic diameter	0.351 mm	0.373 mm
Tube thickness		0.32 mm
Mean flow area/frontal are	0.780	0.129
Total heat transfer area/total volume	886 m^2/m^3	138 m^2/m^3
Fin area/total area	0.845	

(b) Louvered fin radiator

Louvered fin-tube radiator shown in Fig.4.2 considered here is cross flow type and the core portion consists of vertical flat coolant tubes and multi-louvered fins, and its dimension as shown in Table 2 is taken from [61].

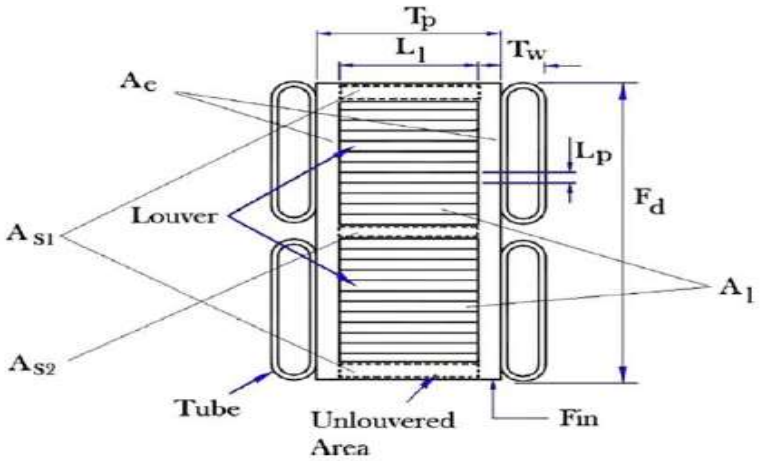

Figure. 4.2: Geometric construction details of louvered fin[61]

Table 4.2: Surface core geometry of tubes and fins (Louvered fin radiator)

Description	Air side	Coolant side
Core Width, W_c	382mm	
Core height, H_c	491mm	
Core depth, F_d	44mm	
Fin metal thickness	0.8mm	
Hydraulic diameter	1.008mm	3.378mm
Tube thickness		0.32mm
Total heat transfer area/total volume	926 m^2/m^3	175 m^2/m^3
Louvered fin parameters	s1 = s2 = 4.1, L_a = 25°, L_p = 0.9, L_h = 1, F_p=2.6, T_p=10, T_w=2.5, L_l=6.8 (all in mm)	

(c) Rectangular fin radiator

Rectangular fin-tube radiator considered here is cross flow type as, which was taken from model of Maruti 800 car. The core portion of the radiator (Fig. 4.3) consists of vertical flat coolant tubes and rectangular fins. All the dimensions, as shown in Table 4.3, have been measured in laboratory

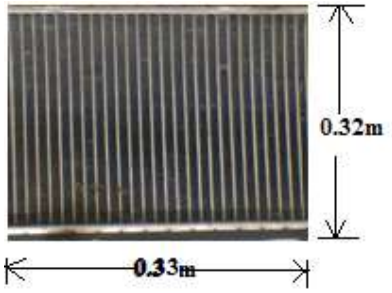

Figure 4.3: Geometric construction of rectangular fin

Table. 4.3: Surface core geometry of tubes and fins (Rectangular radiator)

Description	**Air side**	**Coolant side**
Core Width, W_c	321mm	
Core height, H_c	334mm	
Core depth, F_d	0.2mm	
Hydraulic diameter	2mm	2.4mm
Tube thickness		0.35mm
Total heat transfer area/total volume	$81.35m^2/m^3$	$3.41m^2/m^3$
Tube dimension		$16.2*2*18mm^3$
Number of tubes		33

Based on the assumptions, the overall heat transfer co-efficient, for all types of fins has been calculated by following expression [96]

$$\frac{1}{UA} = \frac{1}{\eta_0 h_a A_o} + \frac{1}{h_{hnf} A_i} \quad (4.1)$$

Where, overall fin efficiency,

$$\eta_0 = 1 - \frac{A_f}{A_o}(1 - \eta_f) \quad (4.2)$$

Air side conductance depends on type of fins (Figs.4.1-4.3)

For wavy fin

Neglecting radiation, the air-side convective heat transfer coefficient is given by,

$$h_a = \frac{j_a G_a c_{p,a}}{Pr_a^{2/3}} \quad (4.3)$$

Where, the correlation for the colburn factor for wavy fin is [148],

$$j_a = 0.836\, Re_a^{-.2309} \left(F_p / F_h\right)^{.1284} \left(F_p / 2A\right)^{-0.153} \left(L_d / L\right)^{-0.326} \qquad (4.4)$$

Surface temperature effectiveness has been calculated by using the fin efficiency, which is given by,

$$\eta_f = \frac{\tanh ml}{ml} \qquad (4.5)$$

Where, for wavy fin,

$$ml = \frac{Fh}{2}\sqrt{2h_a / \left(k_{fin} F_{th}\right)} \qquad (4.6)$$

For air-side heat transfer coefficient calculation in louvered fin, different zones have been considered as shown in Fig.4.2 and individual heat transfer coefficient of each zone has been calculated and combined them. Hence, Air side heat conductance is given by [61],

$$\eta_o h_a A_a = \eta_{f,l} h_l A_l + \eta_{f,s1} h_{s1} A_{s1} + \eta_{f,s2} h_{s2} A_{s2} + h_e A_e \qquad (4.7)$$

Where, zonal heat transfer coefficients are given by,

$$h_l = 0.664 k_a \rho_a u_l \,\mathrm{Re}_l^{-0.5}\, \mathrm{Pr}_a^{0.33} / \mu_a \qquad (4.8)$$

$$h_{s1} = 0.664 k_a \rho_a u_c \,\mathrm{Re}_{s1}^{-0.5}\, \mathrm{Pr}_a^{0.33} / \mu_a \qquad (4.9)$$

$$h_{s2} = 0.664 k_a \rho_a u_c \,\mathrm{Re}_{s2}^{-0.5}\, \mathrm{Pr}_a^{0.33} / \mu_a \qquad (4.10)$$

$$\frac{h_e D_{h_e}}{k_a} = 7.541(1 - 2.61A_r + 4.97A_r^2 - 5.119A_r^3 + 2.702A_r^4 - 0.548A_r^5) \qquad (4.11)$$

For rectangular fin,

$$\eta_f = \frac{\tanh\, ml}{ml} \text{ where, } m = \sqrt{\frac{2\, h_a}{k\, .F_{\mathrm{th}}}} \qquad (4.12)$$

Air-side heat transfer coefficient has been calculated by,

$$h_a = Nu_a * k_a / D_{h,a} \qquad (4.13)$$

Coolant-side heat transfer coefficient can be expressed as:

$$h_f = \frac{Nu_f * k_f}{Dh_f} \quad (4.14)$$

But the correlation for Nu_f depends on type of coolant used

(a)For base fluid

Nu for water, EG, PG and sugarcane juice are given by [96],

$$Nu_f = \frac{(f_f / 2) Re_f Pr_f}{1.07 + 12.7\sqrt{f_f / 2}(Pr_f^{(2/3)} - 1)} \quad (4.15)$$

(b) For nanofluid

The effective density and the effective specific heat of the nanofluid have been evaluated by,

$$\rho_{nf} = (1-\phi)\rho_{bf} + \phi\rho_p \quad (4.16)$$

$$c_{p,nf} = \frac{(1-\varphi)\rho_{bf} * c_{p,bf} + \varphi\ \rho_p * c_{p,p}}{\rho_{nf}} \quad (4.17)$$

Viscosity of nanofluid is given by [96],

$$\mu_{nf} = \mu_{bf}\left(1 - 0.19\phi + 306\phi^2\right) \quad (4.18)$$

The effective thermal conductivity of the nanofluid has been evaluated using following equation [80],

$$k_{nf} = \frac{k_p + 2k_{bf} + 2(k_p - k_{bf})(1+\beta)^3\phi}{k_p + 2k_{bf} - (k_p - k_{bf})(1+\beta)^3\phi} k_{bf} \quad (4.19)$$

Whereas, Nusselt number for nanofluid is expressed as [96]

$$Nu_{nf} = 0.0.2299\left(Re_{nf}^{0.8} - 60\right)Pr_{nf}^{0.4}(1 + 0.32178\varphi^{0.64788}) \quad (4.20)$$

Where, Reynolds number has been calculated using hydraulic diameter.

(c) For Hybrid nanofluids

Thermophysical properties relations for hybrid nano fluids are

$$\phi = \phi_{np1} + \phi_{np2} \quad (4.21)$$

Density of hybrid nanofluid can be expressed as [7]

$$\rho_{hnf} = \phi_{np1} * \rho_{np1} + \phi_{np2} * \rho_{np2} + (1 - \phi) * \rho_{bf} \quad (4.22)$$

Specific heat of nanofluid can be expressed as[7]

$$c_{hnf} = (\phi_{np1}\rho_{np1}c_{p,np1} + \phi_{np2}\rho_{np2}c_{p,np2} + (1-\phi)c_{p,bf})/\rho_{hnf} \quad (4.23)$$

Thermal conductivity of nanofluid can be expressed as [7]

$$\frac{k_{hnf}}{k_{bf}} = \frac{((\phi_{np1}k_{np1}+\phi_{np2}k_{np2})/\phi+2k_{bf}+2(\phi_{np1}k_{np1}+\phi_{np2}k_{np2})-2\phi k_{bf})}{((\phi_{np1}k_{np1}+\phi_{np2}k_{np2})/\phi+2k_{bf}+2(\phi_{np1}k_{np1}+\phi_{np2}k_{np2})-2\phi k_{bf})} \quad (4.24)$$

Viscosity of hybrid nanofluids expresses as [12]

$$\mu_{hnf} = (1 - \frac{\phi}{\phi m})^{-\eta * \phi m}. \quad \text{where, } \phi_m = 0.65 \quad (4.25)$$

where η is the Einstein coefficient, η=2.5, and φ_m=0.65.For calculating the viscosity of nanofluid, φ is the volume concentration of Al_2O_3 nanoparticles in nanofluid; whereas to define this property of hybrid nanofluid (μ_{hnf}), φ must be the overall volume concentration of nanoparticles as indicated in [12].

Nusselt number for nanofluid [80]

$$Nu_{hnf} = 0.0.2299\left(Re_{hnf}^{0.8} - 60\right)Pr_{hnf}^{0.4}(1 + 0.32178\varphi^{0.64788}) \quad (4.26)$$

(d) Radiator performance analysis

Air-side heat capacity rate is given by:

$$C_a = \rho_a u_a H_c W_c c_{p,a} \quad (4.27)$$

Again air-side pressure drop is given by,

$$\Delta p_a = \frac{G_a^{\,2}}{2\rho_{a,i}}\left[\left(1+\sigma^2\right)\left(\frac{\rho_{a,i}}{\rho_{a,e}}-1\right)+f_a\frac{2F_d}{D_{h,a}}\left(\frac{\rho_{a,i}}{\rho_{a,e}}+1\right)\right] \quad (4.28)$$

Then the fan power has been calculated by,

$$P_F = W_c H_c C_{frontal} \Delta p_a / \eta_F \quad (4.29)$$

The coolant-side heat capacity rate is given by,

$$C_f = \rho_f * V_f * c_{p,f} \quad (4.30)$$

Coolant pressure drop is given by:

$$\Delta p_f = \left[G^2{}_f \times f_f \times H_c \right] \Big/ \left[2 \times \rho_f \times \left(D_{h,f} / 4 \right) \right] \quad (4.31)$$

Effectiveness for cross-flow unmixed fluid is given by [52],

$$\varepsilon = 1 - \exp\left[\frac{NTU^{0.22}}{C^*} \exp\left(-C^* NTU^{0.78} - 1 \right) \right] \quad (4.32)$$

Total heat transfer rate,

$$Q = \varepsilon \, C_{min} \, (T_{f,in} - T_{a,in}) \quad (4.33)$$

Coolant pumping power,

$$P_P = V_f \Delta p_f / \eta_P \quad (4.34)$$

Where, the friction factor correlation of nanofluid is expressed as [107],

$$f_f = 0.316 * Re_f^{-0.25} * \left(\frac{\rho_{nf}}{\rho_{bf}} \right)^{0.797} \left(\frac{\mu_{nf}}{\mu_{nf}} \right)^{0.108} \quad (4.35)$$

Now, the performance index can be defined by,

$$PI = \frac{Q}{P_P + P_F} \quad (4.36)$$

Second law based performance criteria of a heat exchanger uses either entropy or exergy as an evaluation parameter [182]. For a radiator, coolant can be taken as incompressible fluid and air can be taken as compressible fluid. Hence, the entropy generation of a radiator can be expressed as:

$$\dot{S}_{gen} = \dot{m}_a \left[c_{pa} \ln \frac{T_{a,e}}{T_{a,i}} - R_a \ln \frac{p_{a,e}}{p_{a,i}} \right] + \dot{m}_f \left[c_{pf} \ln \frac{T_{f,e}}{T_{f,i}} - \frac{p_{a,e} - p_{a,i}}{\rho_f T_{f,mea\,n}} \right] \quad (4.37)$$

Following the methodology adopted in Mishra et al. [182], the entropy generation number ($N_s = \dot{S}_{gen} / C_{\max}$) for radiator can be derived as:

$$N_s = \frac{C_a}{C_{\max}}\left[\ln\left\{1-\varepsilon\frac{C_{\min}}{C_a}\left(1-\frac{T_{f,i}}{T_{a,i}}\right)\right\}-\frac{R_a}{c_{p\,a}}\ln\left\{1-\frac{\Delta p_a}{p_{a,i}}\right\}\right] + \frac{C_f}{C_{\max}}\left[\ln\left\{1+\varepsilon\frac{C_{\min}}{C_f}\left(\frac{T_{a,i}}{T_{f,i}}-1\right)\right\}+\frac{\Delta p_f}{\rho_f c_{pf} T_{f,mean}}\right] \tag{4.38}$$

The exergy loss by the coolant is given by [96],

$$\Delta Ex_f = Q - T_0\left[\dot{m}_f c_{pf}\ln\left(T_{f,i}/T_{f,e}\right)-\dot{m}_f\,\Delta p_f/\left(\rho_f T_{f,mean}\right)\right] \tag{4.39}$$

Whereas, the exergy gain rate by air is calculated by [96],

$$\Delta Ex_a = Q - T_0\left[\dot{m}_a c_{p\,a}\ln\left(T_{a,e}/T_{a,i}\right)+\dot{m}_a R\ln\left(p_{a,i}/p_{a,e}\right)\right] \tag{4.40}$$

Now, the irreversibility is given by,

$$I = \Delta Ex_f - \Delta Ex_a = T_0\dot{S}_{gen} \tag{4.41}$$

If, dimensionless exergy loss define by $I^* = I / Q_{\max}$, then,

$$I^* = \frac{N_s}{C^*}\frac{T_0}{T_{f,i}-T_{a,i}} \tag{4.42}$$

Finally, the second law efficiency is given by,

$$\eta_{II} = \Delta Ex_a / \Delta Ex_f \tag{4.43}$$

Combining Equations (4.36)- (4.42), the following expression can be obtained,

$$\eta_{II} = \frac{\varepsilon - \frac{T_0}{T_{f,i}-T_{a,i}}\frac{C_a}{C_{\min}}\left[\ln\left\{1-\varepsilon\frac{C_{\min}}{C_a}\left(1-\frac{T_{f,i}}{T_{a,i}}\right)\right\}-\frac{R_a}{c_{p\,a}}\ln\left\{1-\frac{\Delta p_a}{p_{a,i}}\right\}\right]}{\varepsilon + \frac{T_0}{T_{f,i}-T_{a,i}}\frac{C_f}{C_{\min}}\left[\ln\left\{1+\varepsilon\frac{C_{\min}}{C_f}\left(\frac{T_{a,i}}{T_{f,i}}-1\right)\right\}+\frac{\Delta p_f}{\rho_f c_{pf} T_{f,mean}}\right]} \tag{4.44}$$

4.1.2 Simulation procedure and validation

For implementing the analysis, an EES code [181] was written for the studied wavy fin, louvered fin and rectangular fin radiators. Thermo-physical and transport properties of both air and coolants have been calculated based on mean temperature. As the exit temperatures are output parameters of simulation, iteration has been done to use of mean temperature based properties. In-built subroutines have been used for the temperature dependent properties of water (for nanofluid also) and air. Web site based data set has been used for the temperature dependent properties of EG and PG.

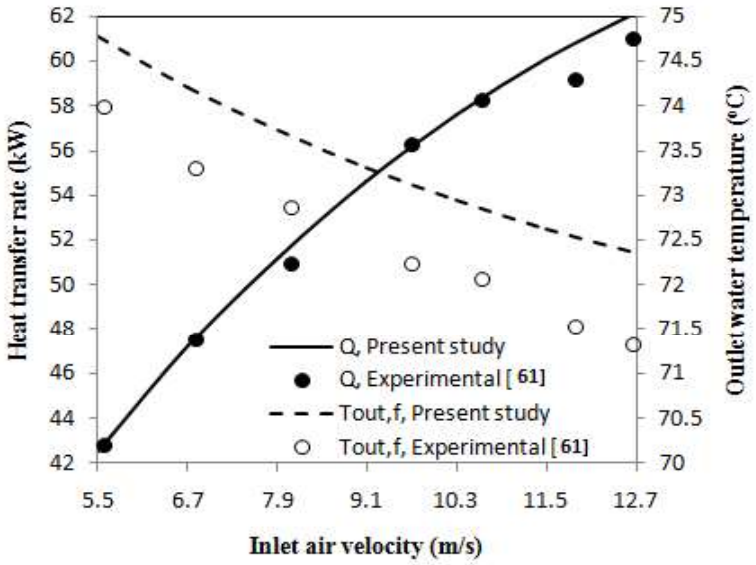

Figure 4.4: Validation of simulation code with experimental data [61] for water

Temperature dependent properties of sugarcane juice have been taken from research work by [179-180]. Properties of alumina nanoparticles have been taken from [96]. Nanoparticle volume fraction has been taken as 1.5%.

The numerical code has been verified with experimental data [61]. A comparison is shown in Fig.4.4, for variations of heat transfer rate and water outlet temperature with inlet air velocity for same geometry and operating

conditions ($T_{in,a}$= 30°C, $T_{in,f}$= 80°C and V_f = 120 l/min). Similar trend has been observed and showed maximum 3% and 2% deviations between the predicted and experimental data for heat transfer rate and water outlet temperature, respectively.

4.1.3 Results and discussions

4.1.3.1 Wavy fin radiator analysis with various coolants

(a) With base fluid

Comparison of heat transfer coefficient, heat transfer rate and effectiveness for various coolants are shown in Figs. 4.5-4.7. As shown, sugarcane is having higher heat transfer coefficient at higher temperature (approximately above 60°C), it yields higher heat transfer rate of 49 kW,followed by water, EG and PG at coolant flow rate of 120 l/min in wavy fin radiators. Also,sugarcane juice coolant yeild higher effectiveness of 45% as compared to other coolants i.e water, EG and PG as coolants for radiators.

.

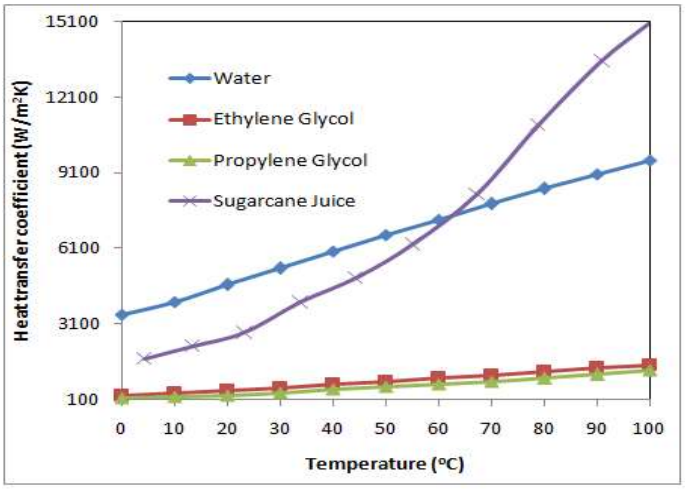

Figure 4.5: Variation of heat transfer coefficient with temperature

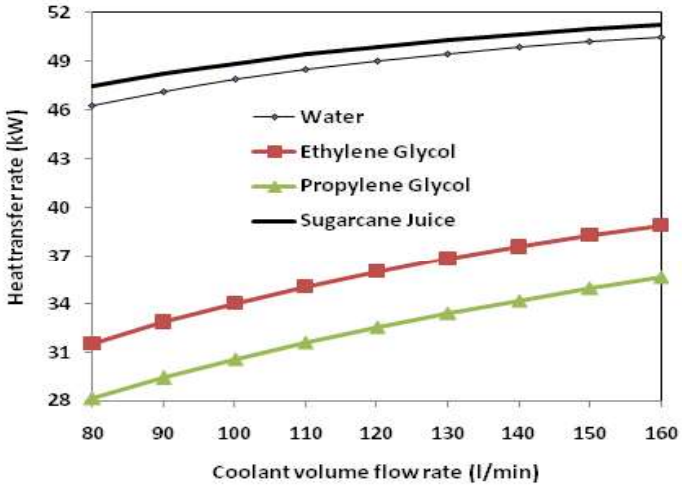

Figure 4.6: Heat transfer rate with coolant flow rate

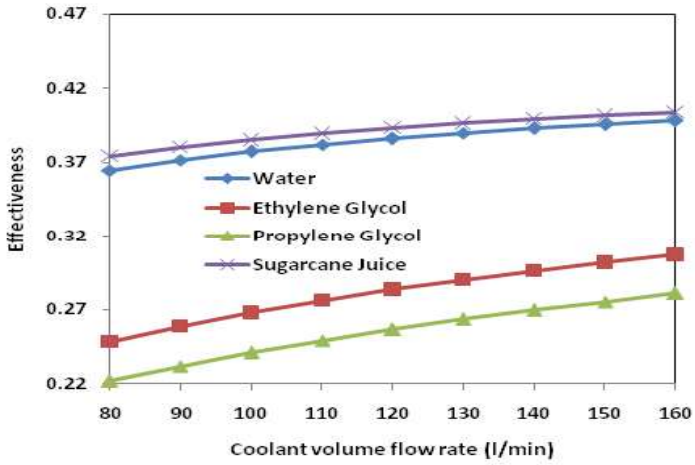

Figure 4.7: Effectiveness with coolant flow rate

The required pumping power is higher for PG shown in Fig 4.8, having the value of 2.6W and sugarcane juice coolant yields lower pumping power of 0.8W to pump a coolant flow rate of 120 l/min in wavy fin radiator and follwed by other coolants as EG and alumina nanofluids. Lower pressure drop in sugarcane juice results in lower pumping power as compared to other coolants.

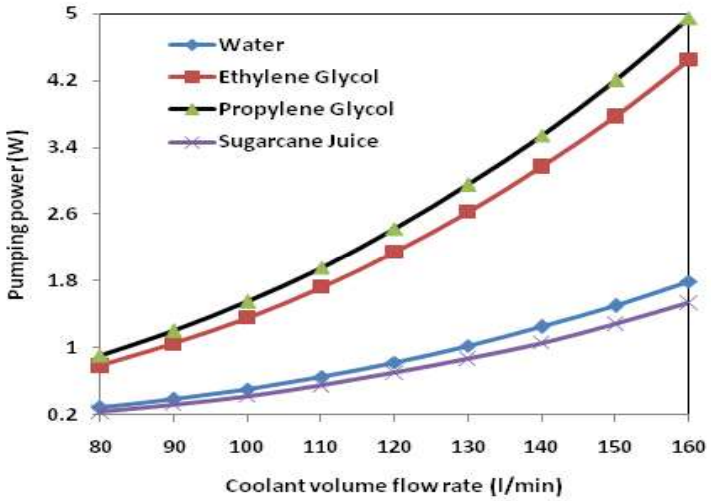

Figure4.8: Pumping power with coolant flow rate

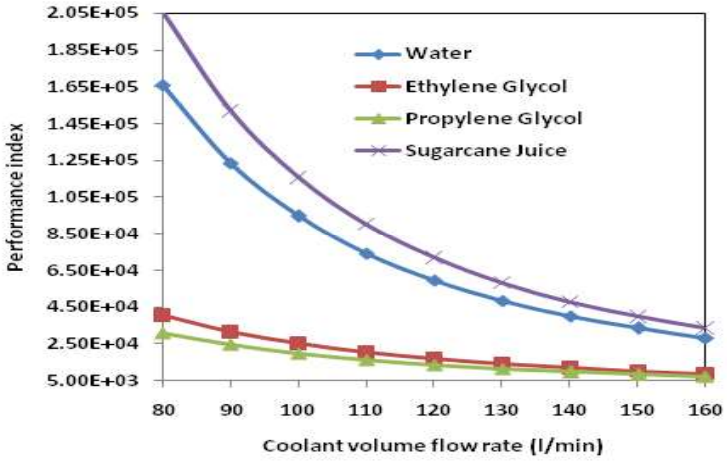

Figure 4.9: Performance index with coolant flow rate

The performance index is highest for sugarcane juice coolant due to lower pumping power and PG coolants having lowest performance index of at coolant flow rate of 120l/min in wavy fin radiators as compared to other coolants i.e EG ,water as shown in Fig.4.9.

Sugarcane juice coolant having higher second law efficiency of 22% shown in Fig.4.10 and PG having lower second law efficiency of 12% at a coolant

flow rate of 120 l/min as compared to other coolants i.e alumina nano fluids, water, ethylene glycol as coolants for wavy fin radiator

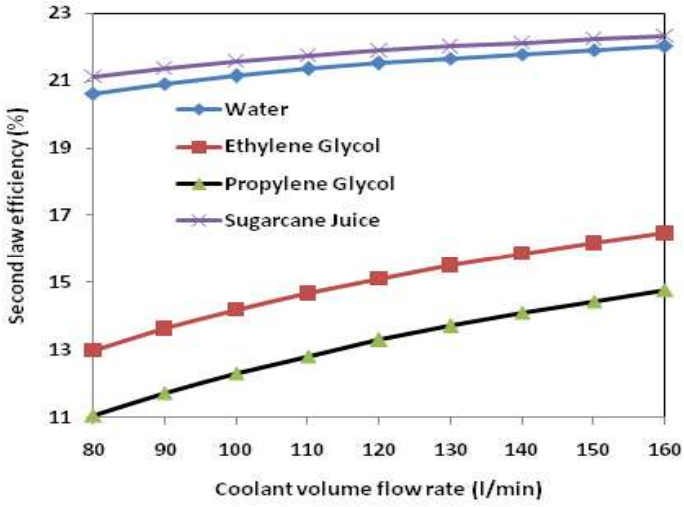

Figure 4.10: Second law efficiency with coolant flow rate

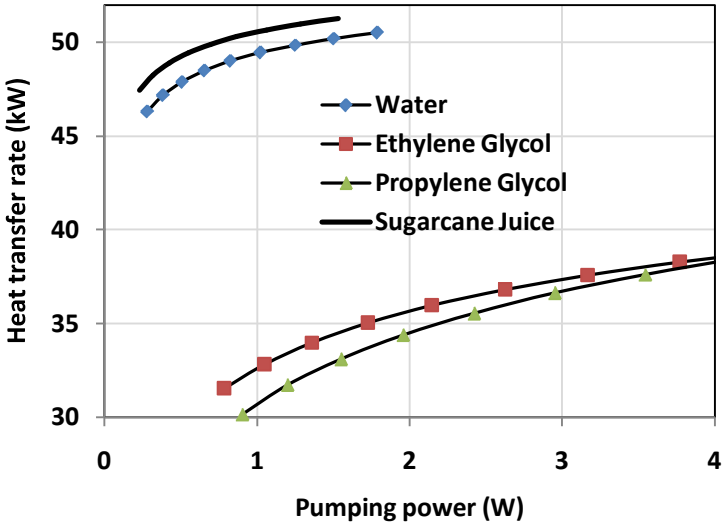

Figure 4.11: Heat transfer rate and pumping power variation

As shown in Fig.4.11, at pumping power approximately 1.5W, sugarcane juice has higher heat transfer rate in wavy fin as compared to other coolants. Sugarcane juice coolant having maximum heat transfer rate as compared to other

coolants i.e water,ethylene glycol, PG with pumping power.The comparisons for the performance of radiator with various base fluid have been shown in Table-4.4.

Table 4.4 Performance of radiator with various base fluid (Wavy fin)

Parameters	Water	EG	PG	Sugarcane juice	Water+ 25% EG	Water +25%PG
Heat transfer rate (kW)	56.96	39.85	35.56	58.01	54.54	56.92
Effectiveness (%)	44.88	31.40	28.02	45.70	42.97	44.85
Pumping Power (W)	1.526	3.921	4.361	1.350	1.961	1.449
Performance index	37334	10164	8155	42963	27812	39276
Second law of efficiency (%)	25.96	17.88	15.71	26.33	24.77	25.89

(b) With nanofluids

The heat transfer performance of water-PG brine (about 25% PG) at an optimum brine composition yielding maximum heat transfer performance. Furthermore, the 25% brine solution also increases operating temperature range (higher boiling point and lower freezing point). For the simulation, coolant inlet temperature, air inlet temperature and air frontal velocity have been taken as 90^{o}C, 30^{o}C and 10m/s, respectively.

Variations of the heat transfer rate, effectiveness, pressure drop and pumping power with nano particle volume fraction are predicted in Figs. 4.12-4.15.The heat transfer rate of 25% PG brine based Ag nanofluid highly increases due to high heat transfer coefficient. As compared to PG brine,1% volume fraction of 25% PG brine based Ag nanofluid has higher heat transfer rate and effectiveness and followed by CuO , $Al_2O_3$and $TiO_{2,.}$ Pressure drop of all studied nanofluids increases with increase in volume fraction due to increase in viscosity.

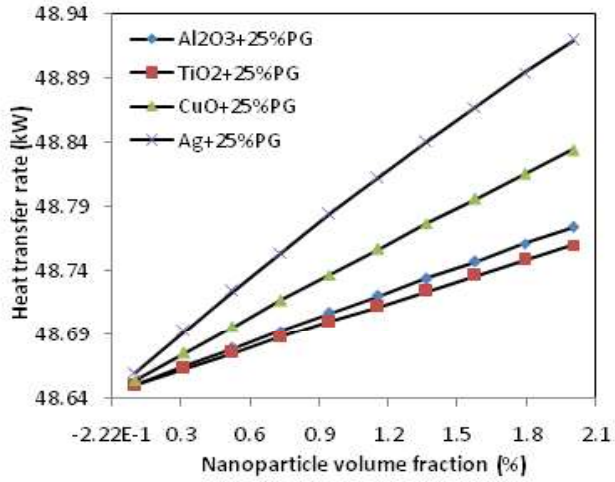

Figure. 4.12: Heat transfer variation with particle volume fraction

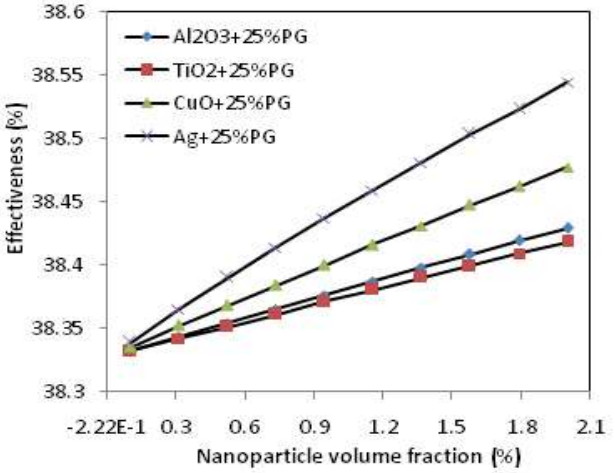

Figure. 4.13: Effectiveness variation with particle volume fraction

However, the pressure drop decreases for 25%PG based Ag nanofluid and hence required less pumping power and followed by CuO, TiO_2, Al_2O_3 nanofluids as coolant for wavy fin automotive radiator.

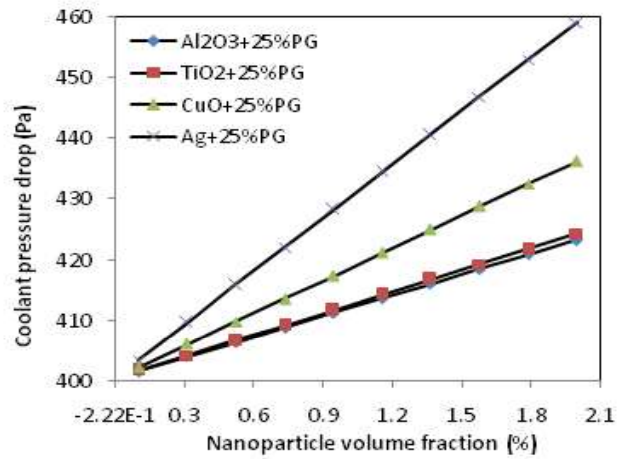

Figure 4.14: Pressure drop variation with particle volume fraction

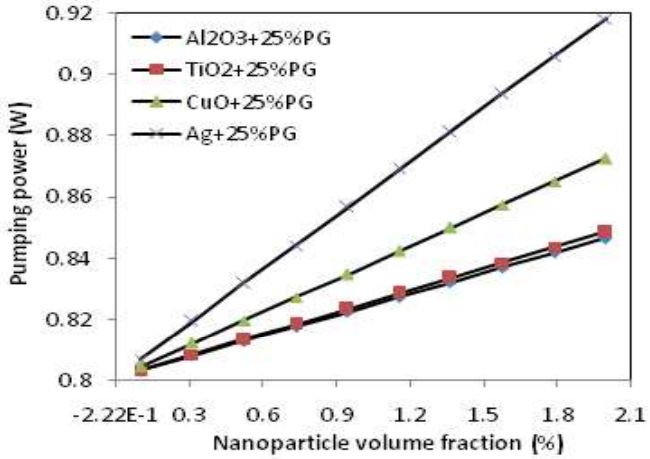

Figure 4.15: Pumping power variation with particle volume fraction

Second law efficiency increases with increase in particle volume fraction for all studied PG based nanofluid coolants as shown in Fig.4.16. This can be attributed by the fact that with increase in particle volume fraction , the effective temperature difference decreases due to improvement of heat transfer performance and hence irreversibility decreases. However, PG brine based Ag nanofluid has higher second law efficiency of 21.43% , followed by CuO, TiO_2 and Al_2O_3 nanofluids as coolant for radiator

Performance characteristic of PG brine based coolants is illustrated in Fig. 4.17. For same heat transfer capacity, the pumping power requirement is significantly lower for PG based Ag nanofluids followed by TiO_2, Al_2O_3 and CuO nanofluids. Similarly, for same pump power supply, heat transfer rate is significantly higher with PG based Ag nanofluids.

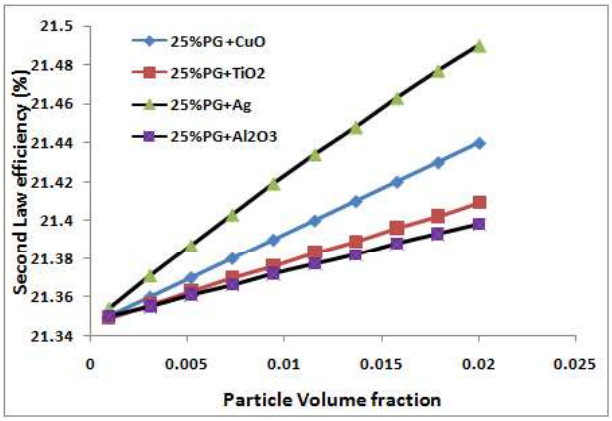

Figure 4.16: Second law efficiency with particle volume fraction

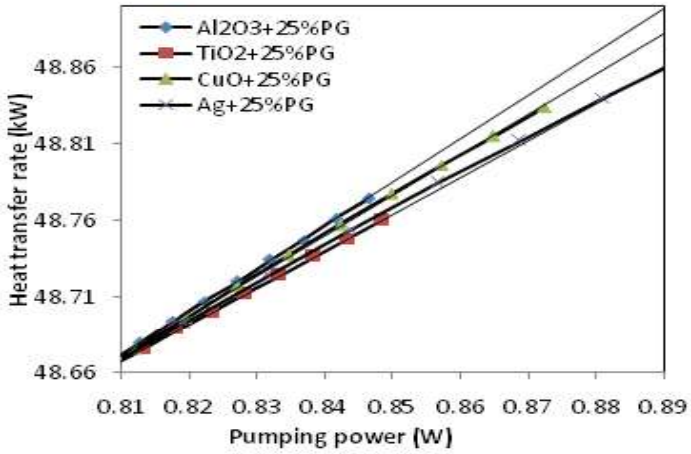

Figure. 4.17: Performance graph (heat transfer rate with pumping power)

Compared to conventional coolant (PG brine), the coolant flow rate and pumping power reduce significantly by 3.6% to 2.9% and 3.5% to 1.1% respectively, by using PG brine based Ag nanofluid and followed by CuO, Al_2O_3

and TiO_2 nanofluids, for same cooling capacity and radiator size as shown in Figs. 4.18-4.19.

Reductions of coolant flow rate and pumping power lead to decrease of coolant cost and increase of overall engine efficiency or decrease of fuel consumption, respectively.On the other hand, for same cooling capacity and volume flow rate, the radiator size reduces by 3.7% to 1.5%, by using PG brine based Ag, followed by CuO, Al_2O_3 and TiO_2 nanofluids. Reduction of radiator size may lead to compactness as well as decrease of radiator weight and cost.

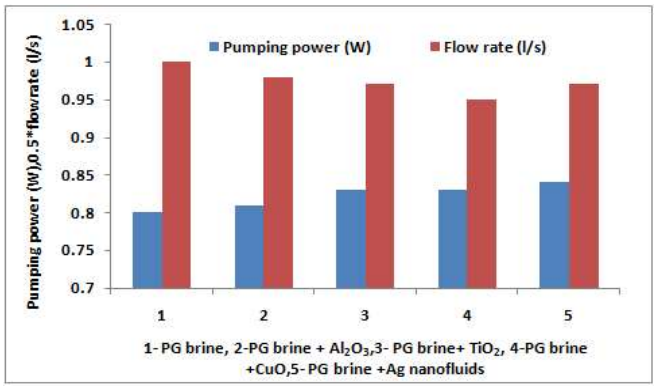

Figure 4.18: Comparison for same heat transfer rate and radiator size

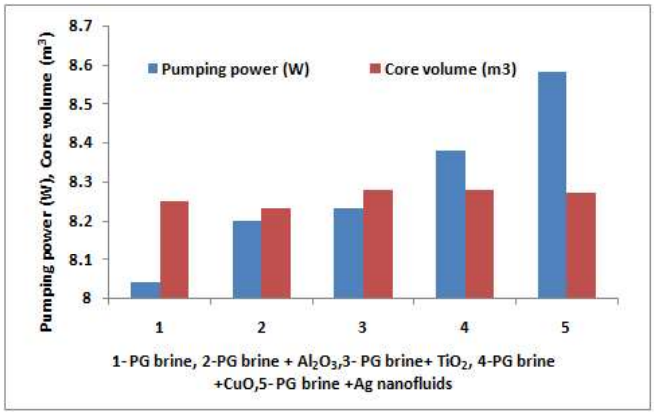

Figure 4.19: Comparison for same heat transfer rate and mass flow

(c) With hybrid nanofluids

Variations of the heat transfer rate, effectiveness, pumping power, pressure drop with various volume fraction of Fe_2O_3, CuO, Cu, Ag hybrid

nanofluids within 0 to 1 % in volume fraction of Al_2O_3 nanofluid are predicted in Figs. 4.20-4.23, with coolant volume flow rate of 120 l/min. Results show that among all studied hybrid nanofluids, 1% Ag hybrid nanofluid (0.5% Ag/5% Al_2O_3) has higher effectiveness and heat transfer rate of 5% and 8% respectively, with comparison to 1% volume fraction Al_2O_3 nanofluid and is followed by 1% volume fraction (50/50) of Cu,CuO,Fe_2O_3,TiO_2 hybrid nanofluids. Due to higher heat transfer coefficient, heat capacity and lower dynamic viscosity, Ag hybrid nanofluid resuls higher heat transfer rate and gradually decreases with increases in volume fraction of Al_2O_3 from 0 to 1% in hybrid nanofluids.

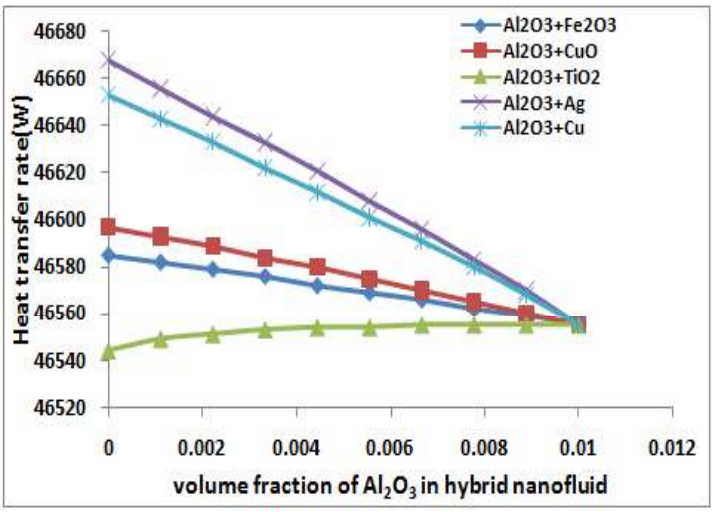

Figure 4 .20: Heat transfer variation with (0-1%) Al_2O_3 hnf

Similarly pressure drop for PG brine based Ag hybrid nanofluid increased by 2% and is followed by Cu, CuO, Fe_2O_3 and TiO_2 hybrid nanofluids as compared to 1% volume fraction Al_2O_3 nanofluid. On the other hand, due to the increase in Reynolds number, pumping power for PG brine based Ag hybrid nanofluid is 2.5% higher and followed by Cu, CuO, Fe_2O_3 and TiO_2 hybrid nanofluids as compared to 1% volume fraction Al_2O_3 nanofluid. But pumping

power decreases gradually with increases in volume fraction of Al_2O_3 from 0 to 1% as coolant for wavy fin automotive radiator.

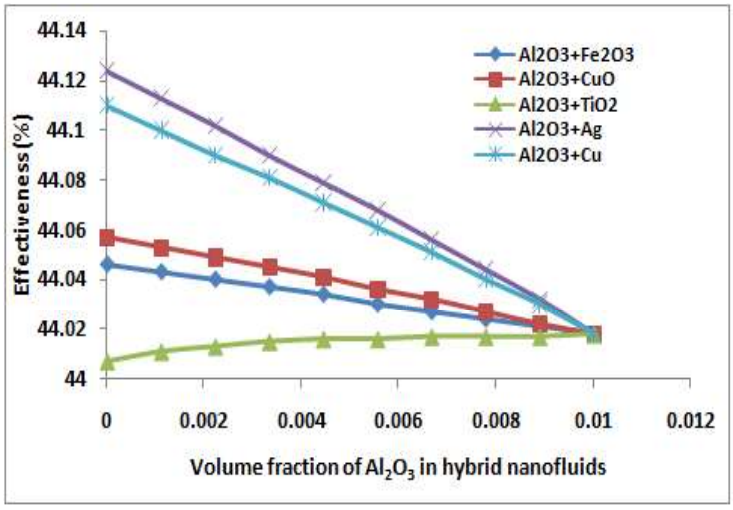

Figure 4.21: Effectiveness variation with (0-1%) Al_2O_3hnf

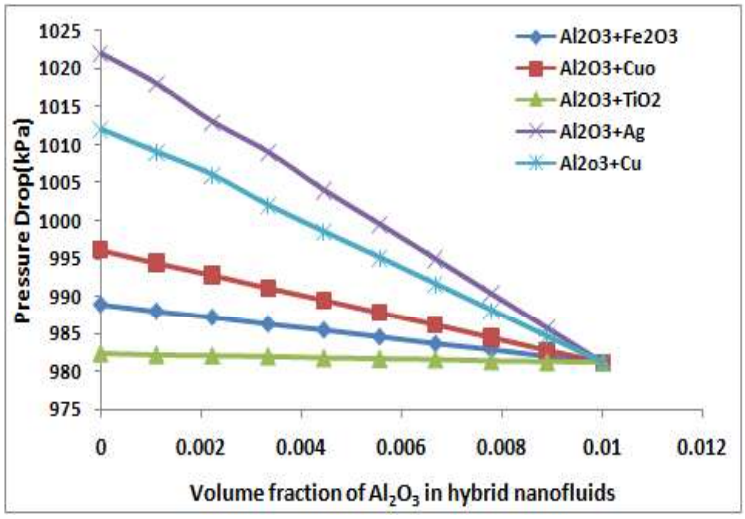

Figure 4.22: Pressure drop variation with (0-1%) Al_2O_3 hnf

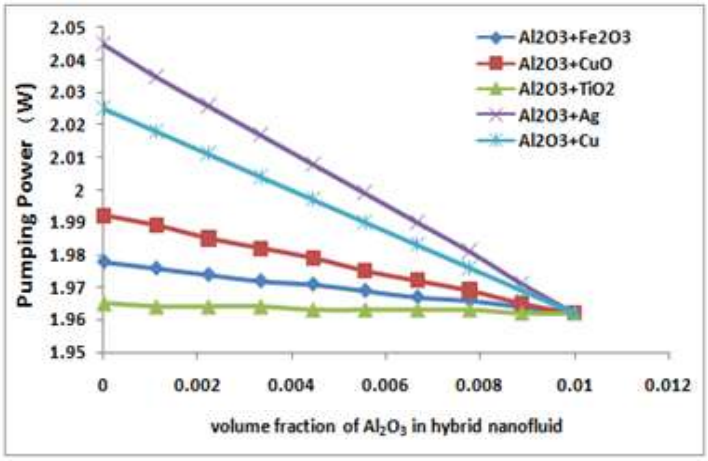

Figure 4.23: Pumping power variation with (0-1%) Al_2O_3hnf

Figs. 4.24- 4.25, show that, for the same radiator size and same heat transfer rate, coolant flow rate decreases by 2.5% and pumping power increased by 1.3 % for 1% vol. fraction (0.5% Al_2O_3 and 0.5% TiO_2) hybrid nanofluid as compared to 1% vol. fraction Al_2O_3 nanofluid. Similarly for the same coolant flow rate and same heat transfer rate, radiator size reduced by 1.5% and pumping power increases 2.7% for (0.5%Al_2O_3/0.5%Ag) hybrid nanofluids as compared to 1% vol. fraction Al_2O_3 nanofluid.

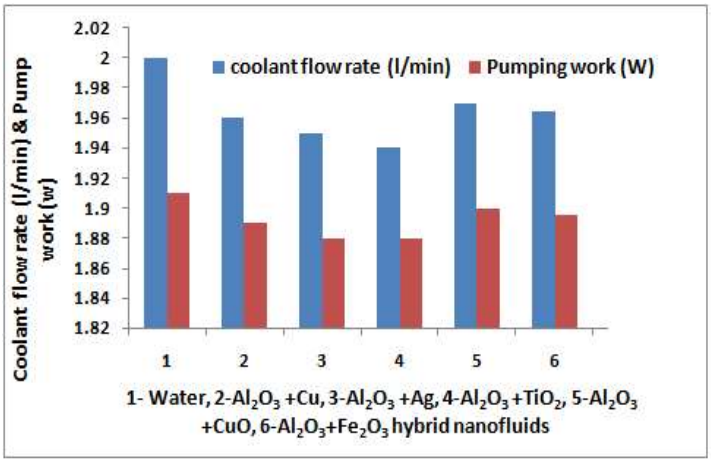

Figure 4.24: Comparison for same heat transfer rate and radiator size

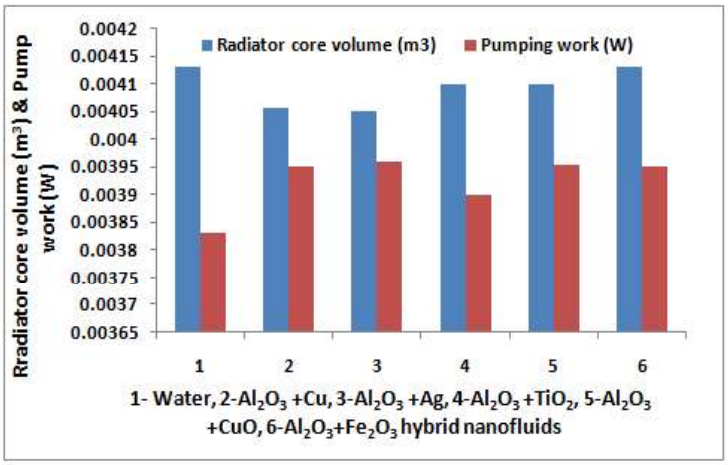

Figure 4.25: Comparison for same heat transfer rate and mass flow rate

Reduction of radiator size may lead to compactness as well as decrease of radiator weight and cost. As discussed earlier, values of above effects may change by using other hybrid nanofluids.

4.1.3.2 Louvered fin radiator performance with various coolants

(a) For base fluids

The sugarcane juice is better than above mentioned coolants in terms of both heat transfer and pressure drop at higher temperature. In general, the automotive radiator is operated at coolant mean temperature of above 60^{o}C and hence it is expected to get better performance with sugarcane juice. This interesting fact has motivated the present simulation study using sugarcane juice as automotive engine coolant.

Variations of the heat transfer rate, effectiveness, pumping power, performance index and second law efficiency with various coolant volume flow rate are shown in Figs. 4.26-4.30

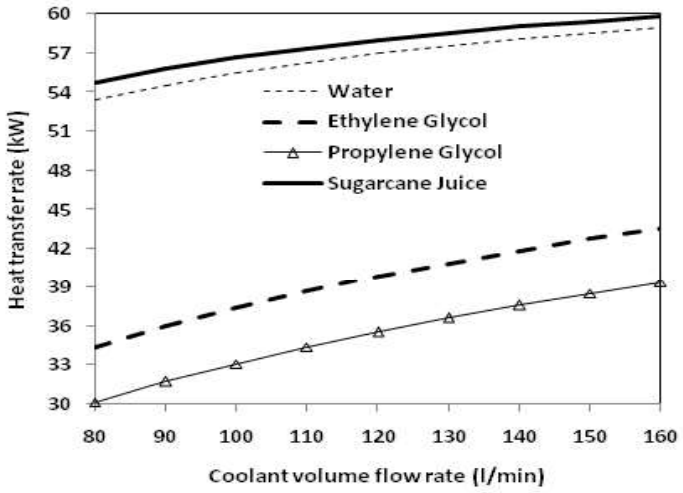

Figure 4.26: Variation of heat transfer rate with CFR

It has been observed that heat transfer rate, effectiveness and pumping power go on increasing with coolant flow rate due to dual effects of heat transfer coefficient and heat capacity increments. However, sugarcane juice yields slightly better heat transfer rate and effectiveness than water whereas, significantly better than EG and PG mainly due to lower dynamic viscosity.

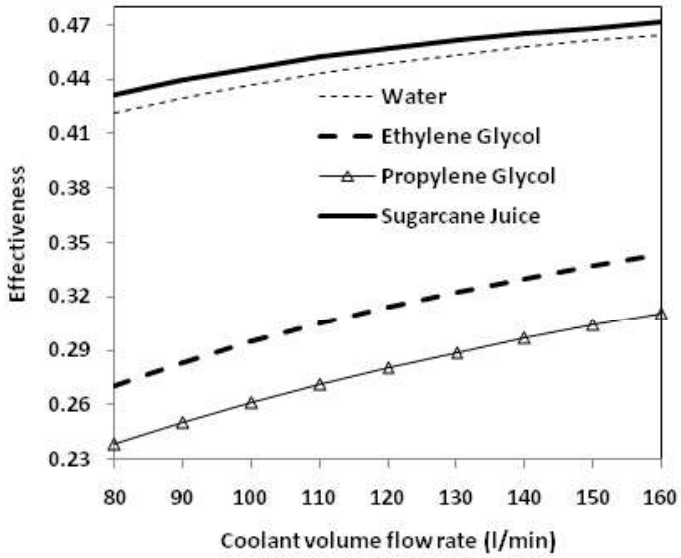

Figure 4.27: Variation of heat exchanger effectiveness with CFR

On the other hand, due to same reason, pumping power of sugarcane juice is slightly lower than water, whereas significantly lower than EG and PG. As a result, sugarcane juice yields slightly better performance index and second law efficiency than water whereas significantly better than EG and PG. However, performance index highly decreases (as the effect of flow rate on pumping power is more predominant than that on heat transfer rate), whereas second law efficiency increases with increase in coolant volume flow rate for all studied coolants.

Performance characteristic of various coolant is illustrated in Fig.4.31. For same heat transfer capacity, the pumping power requirement is minimum with sugarcane juice, followed by water, EG and PG. Similarly, for same pump power supply, heat transfer rate is maximum with sugar cane juice, followed by water, EG and PG.

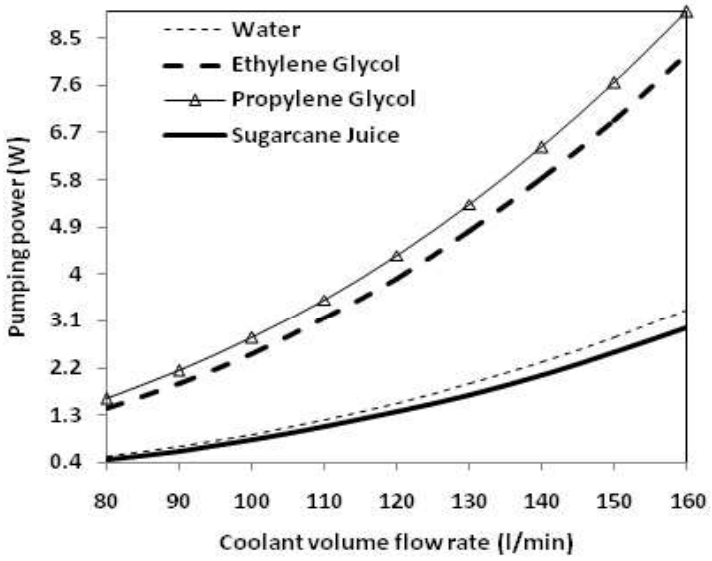

Figure 4.28: Variation of pumping power with CFR

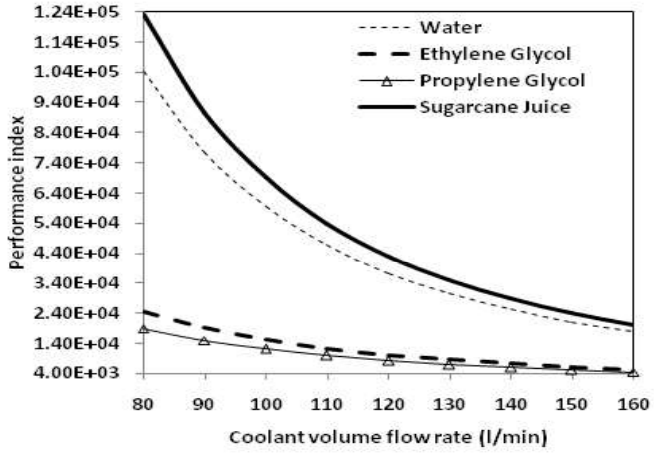

Figure 4.29: Variation of performance index with CFR

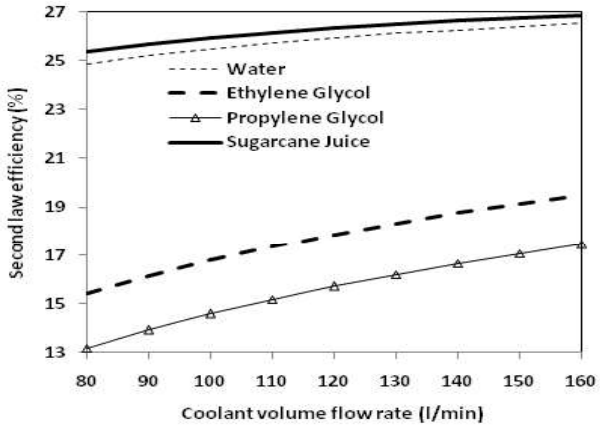

Figure 4.30: Variation of second law efficiency with CFR

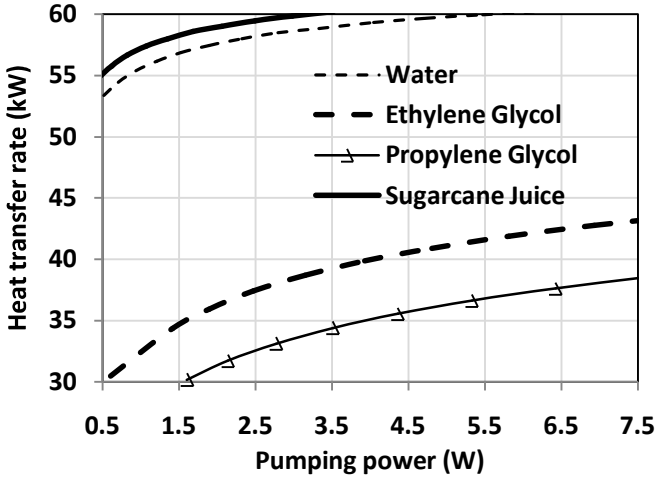

Figure 4.31: Performance graph (heat transfer rate with pumping power)

Variations of heat transfer rate and effectiveness with EG or PG mass fraction in water based brines are shown in Fig.4.32. With increase in mass fraction, the heat transfer rate and effectiveness gradually decrease for EG, whereas, for PG, it seems to be increases initially, and then decreases by yielding some maximum values corresponding to optimum mass fraction of about 25%. This abnormal behavior of perfomance with PG mass fraction may be due to the typical change of dynamic viscosity. It may be noted that the performance values are similar to that with pure water. Due to same reason (viscosity change behavior), pumping power yields minimum value at about 25%, whereas, it increases continuously for EG. As a result, performance index decreases monotonically for EG with mass fraction whereas decreases, increases and again decreases with PG mass fraction yielding maximum value at about 25% mass fraction.

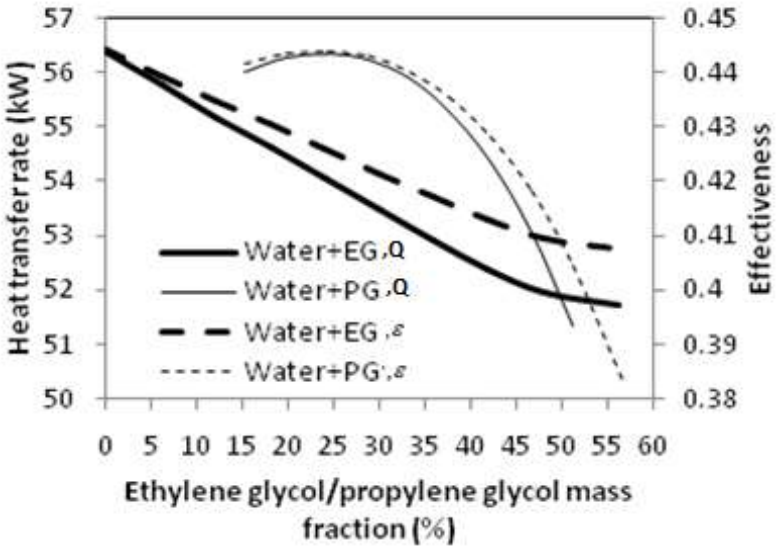

Figure 4.32: Variation of heat transfer rate and effectiveness for brines

Table 4.5 : Performance comparison of various heat transfer fluids (coolants)

Parameters	Water	EG	PG	Sugarcane Juice	Water + 25% EG	Water + 25% PG
Heat transfer rate (kW)	56.96	39.85	35.56	58.01	54.54	56.92
Effectiveness (%)	44.88	31.40	28.02	45.70	42.97	44.85
Pumping power (W)	1.526	3.921	4.361	1.350	1.961	1.449
Performance index	37334	10164	8155	42963	27812	39276
Second law efficiency (%)	25.93	17.88	15.71	26.33	24.77	25.89

Comparison of various fluids are summerized in Table 4.5 with coolant volume flow rate of 120 lpm and air frontal velocity of 10m/s. As shown, sugarcane juice yields maximum performance followed by water+25%PG and water. Recently many studies showed 5-10% radiator performance improvement using nanofluids [95-99]. Hence, it seems to be similar radiator performance by using nanofluids and sugarcane juice. Furthermore, there is an another opportunity to use water+25%PG based nanofluids for performance improvement of radiator. However, both sugarcane juice and nanofluids have some challenges such as long term stability to use in radiator.

Reduction in size and weight of the radiators are among the achievements of this type of researches. In addition to reducing the production cost, better designation of cars are possible when the radiator becomes smaller in size. On the other hand, better cooling has positive effects on fuel consumption and the amount of fuel consumption decreases.

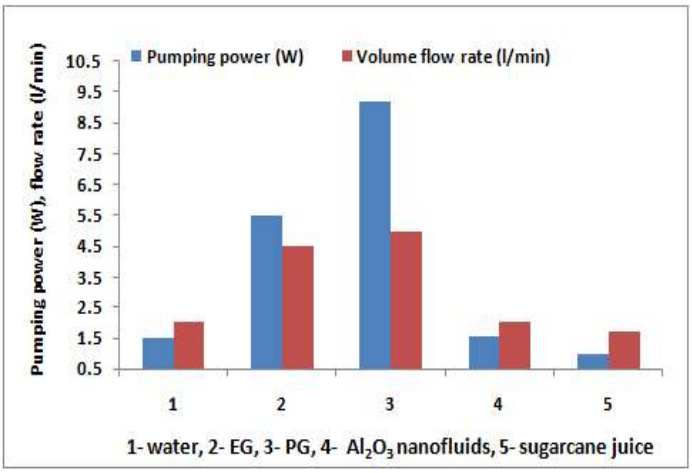

Figure 4.33: Comparison for same heat transfer rate and radiator size

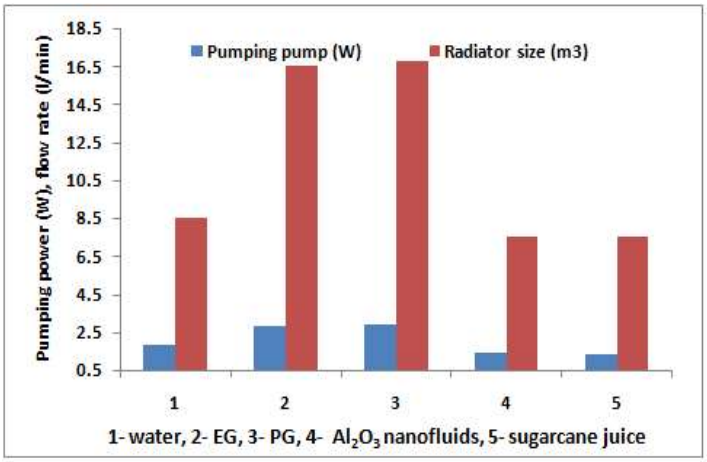

Figure 4.34: Comparison for same heat transfer rate and mass flow rate

Compared to water, the coolant flow rate and pumping power reduce by 13% and 41% respectively, by using sugarcane juice, whereas, only 5% both by using alumina nanofluid for same cooling capacity and radiator size (Fig.4.33). Reductions of coolant flow rate and pumping power lead to decrease of coolant cost and increase of overall engine efficiency or decrease of fuel consumption, respectively. On the other hand, for same cooling capacity and mass flow rate, the radiator size and pumping power reduce by 2.5% and 13.5%, respectively, by using sugarcane juice, whereas, about 2% both by using alumina nanofluid

compared to water (Fig.4.34). Reduction of radiator size may lead to compactness as well as decrease of radiator weight and cost. As discussed earlier, values of above effects may change by using other nanofluids.

(d) For hybrid nanofluid

. Variations of the heat transfer rate, effectiveness, pressure drop and pumping power for hybrid nanofluids in 0 to 1 % in volume fraction of Al_2O_3 are predicted in Figs.4.35-4.38. Results show that the heat transfer and effectiveness of PG brine based Ag hybrid nanofluid are 48.4 kW, 38.10% respectively, followed by Cu, CuO, Fe_3O_4 and TiO_2 hybrid nanofluids and gradually decreases with increases in volume fraction of Al_2O_3 from 0 to 1% in hybrid nanofluids. Pressure drop for PG brine based Ag hybrid nanofluid increased by 4.7% as compared to base fluid and followed by Cu, CuO, Fe_3O_4 and TiO_2 hybrid nanofluids. Pumping power for PG brine based Ag hybrid nanofluid is 4.6% higher and followed by Cu, CuO, Fe_3O_4andTiO_2 hybrid nanofluids. But it decreases gradually with increases in volume fraction of Al_2O_3 from 0 to 1% as coolant for wavy fin automotive radiator.

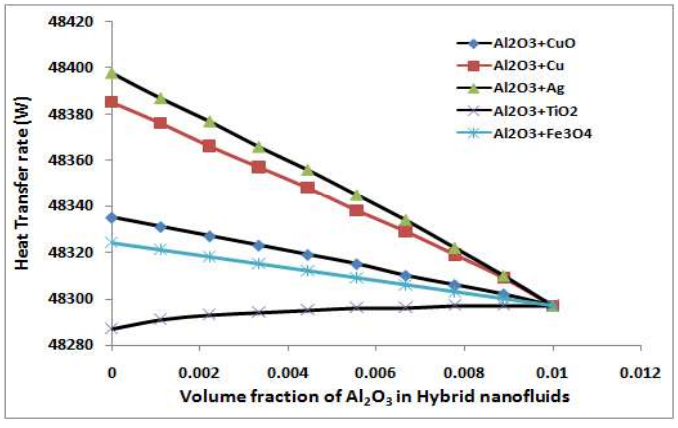

Figure.4.35: Heat transfer variation with (0-1%) Al_2O_3 hnf

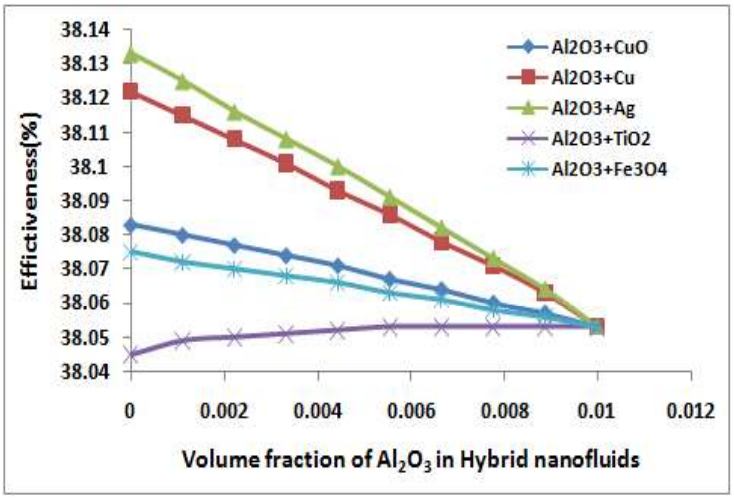

Figure.4.36: Effectiveness variation with (0-1%) Al_2O_3hnf

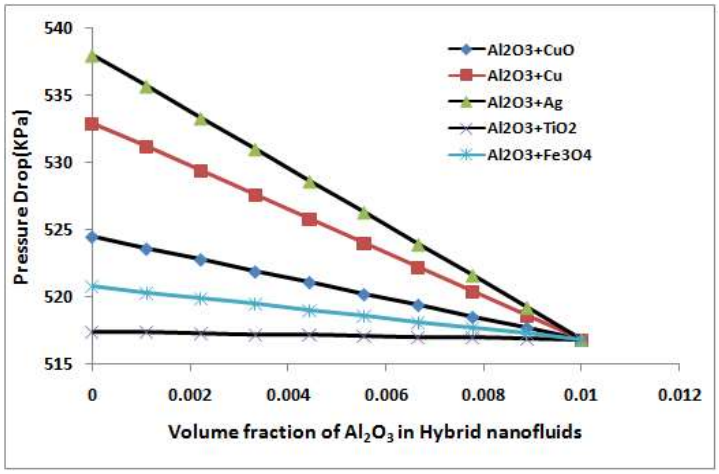

Figure 4.37: Pressure drop variation with (0-1%) Al_2O_3 hnf

However, as shown in Figs. 4.39-4.40, for the same radiator size and same heat transfer rate. Coolant flow rate decreases by 1.5% and pumping power decreased by 1.45 % for (Al_2O_3+ Cu) hybrid nanofluids as compared to base fluid PG brine. Similarly for the same coolant flow rate and same heat transfer rate, radiator size reduced by 2.8% and pumping power increases 3.98% for (Al_2O_3+ Ag) hybrid nanofluids as compared PG brine.

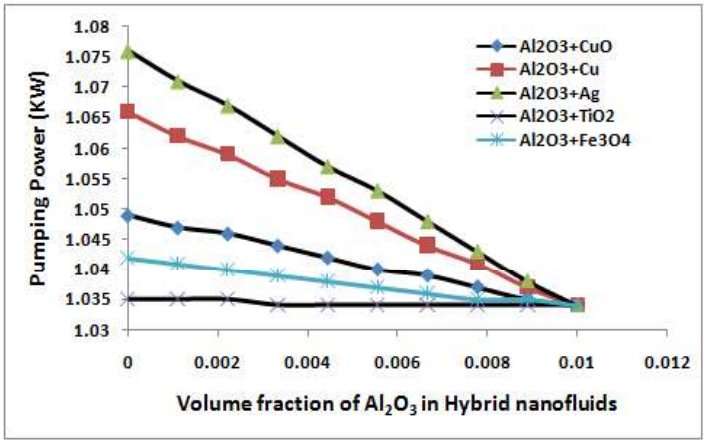

Figure 4.38: Pumping power variation with (0-1%) Al_2O_3hnf

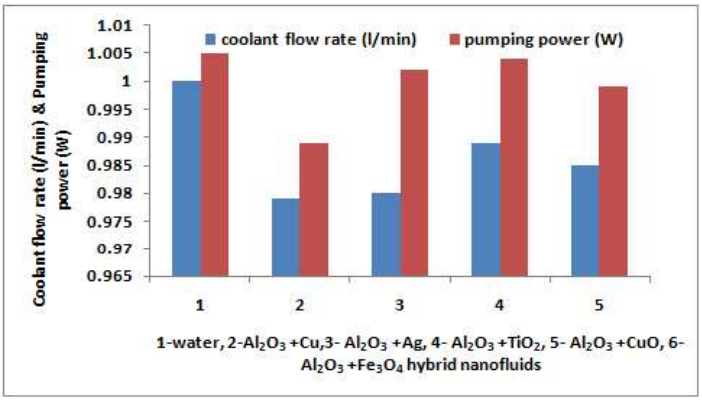

Figure 4.39: Comparison for same heat transfer rate and radiator size

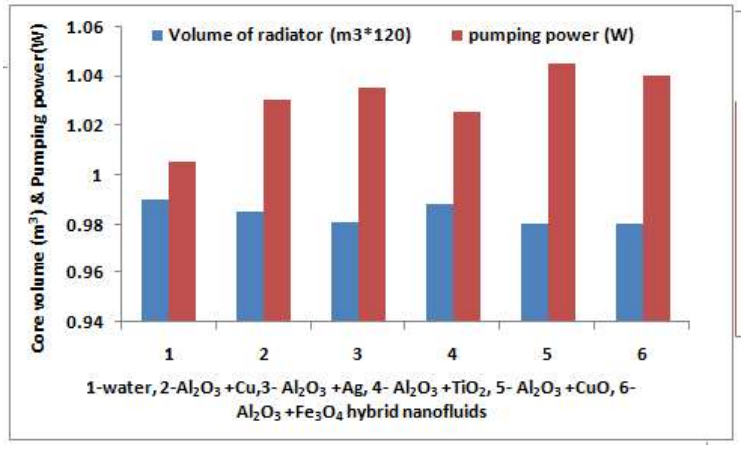

Figure 4.40: Comparison for core volume and pumping power

Performance comparison of various hybrid nanofluids as radiator coolants has been shown in Table 4.6

Table 4.6 : Performance comparison of various hybrid nanofluids (ϕ=1%)

Parameters	(Ag+ Al_2O_3)hnf	(Cu+ Al_2O_3)hnf	(CuO+ Al_2O_3)hnf	(Fe_3O_4 + Al_2O_3)hnf	(TiO_2+ Al_2O_3)hnf
Effectiveness (%)	38.10	38.09	38.07	38.06	38.05
Pressure Drop(kPa)	528	526	521	519	517
Pumping Power(W)	1.056	1.052	1.041	1.038	1.034
Heat transfer rate (kW)	48.39	48.38	48.33	48.32	48.30

4.1.3.3 Performance with rectangular fin for various coolants

(a) Performance with new coolant Optimum PG brine (25% PG brine)

The effects of water based ethylene glycol and PG brine concentrations on the heat transfer rate, pumping power, effectiveness and performance index considered rectangular fin automotive radiator are predicted in Figs.4.41-4.42. With increase in concentration, the heat transfer rate and effectiveness gradually decrease for EG, whereas, for PG, it seems to be decreases initially, then increases and again decreases by yielding some maximum values corresponding to optimum mass fraction of about 25%. Brine concentration of 25% PG results highest performance index with lowest pumping power. It may be noted that this performance values of 25% PG brine are similar to the that with pure water. However, pumping power increases with increase concentration of ethylene glycol due to higher friction factor. This abnormal behavior of perfomance with PG concentration may be explained as follows. PG is highly soluble in water, and readily metabolized by microbes and higher organisms once released into the environment. The biodegradation process requires oxygen; therefore, dissolved oxygen (DO) concentrations in receiving water may be negatively impacted

following a large PG release. Corrosion inhibitor additives may also cause adverse effects to the biodegrading microorganisms, thereby slowing the degradation process. Researchers showed that the PG based heat transfer fluid containing tolytriazole in water had a degradation rate approximately three times lower (slower) than for pure PG [23]. 25% PG brine solution has lower pumping cost, higher heat transfer efficiency and excellent corrosion protection. Glycols are corrosive to most metals. So at higher concentration above 25% PG brine solution, it oxidizes to form acids of high pH which is corrosive. Also, due to slush creation, a PG and water solution should not be used close to freezing points.

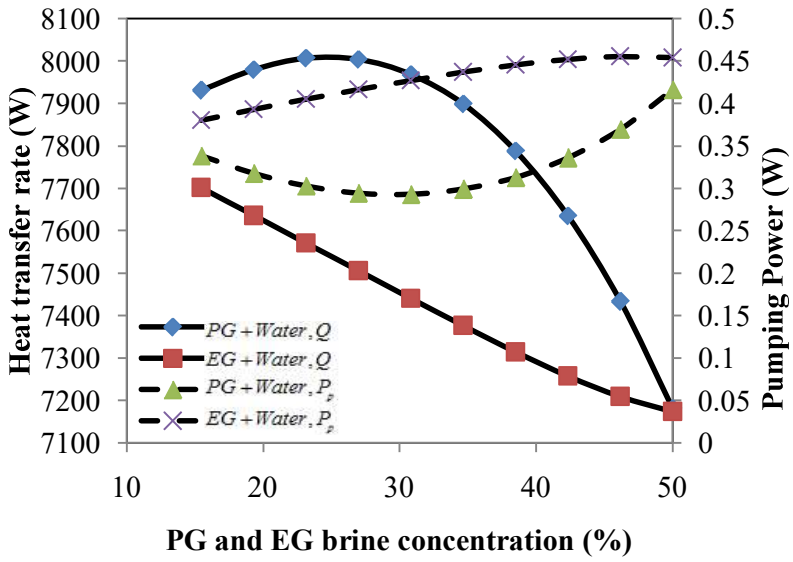

Figure 4.41: Heat transfer rate and pumping power with brine concentration

With the increase in concentration of PG, the viscosity increases due to the formation of gelled fluids at higher temperature range which results low resistance to mixing and also decreases the heat transfer rate. Hence, a minimum concentration of 25% PG brine has been recommended for most applications to provide adequate burst protection and corrosion protection [23].

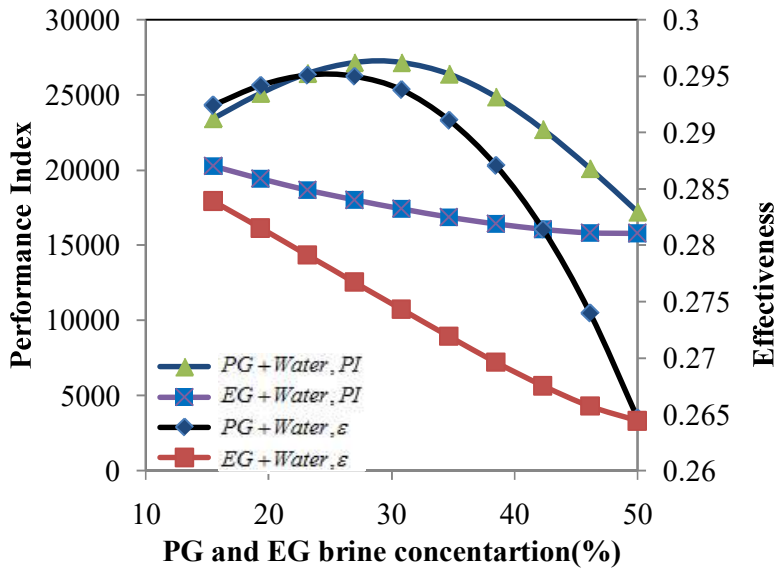

Figure 4.42: Performance index and effectiveness with brine concentration

Due to better heat transfer and lowest pressure drop, optimum (25%) PG brine yields minimum irreversibility whereas the energetic performance monotonically decreases with EG concentration. For foregoing discussion, performances have been evaluated at 25% concentration for both EG and PG.

Comparisons of heat transfer rate, pumping power, effectiveness and performance index for water, 25% EG brine and 25% PG brine are shown in Figs. 4.43- 4.44 for frontal air velocity of 10m/s. The heat transfer rate for water and optimum PG brine are nearly same and 50% higher as compared to 25% ethylene glycol brine and gradually increases with coolant flow rate due to higher effectiveness and higher heat transfer coefficient. Similarly pumping power and pressure drop both are minimum for water and optimum PG brine due to lower friction.

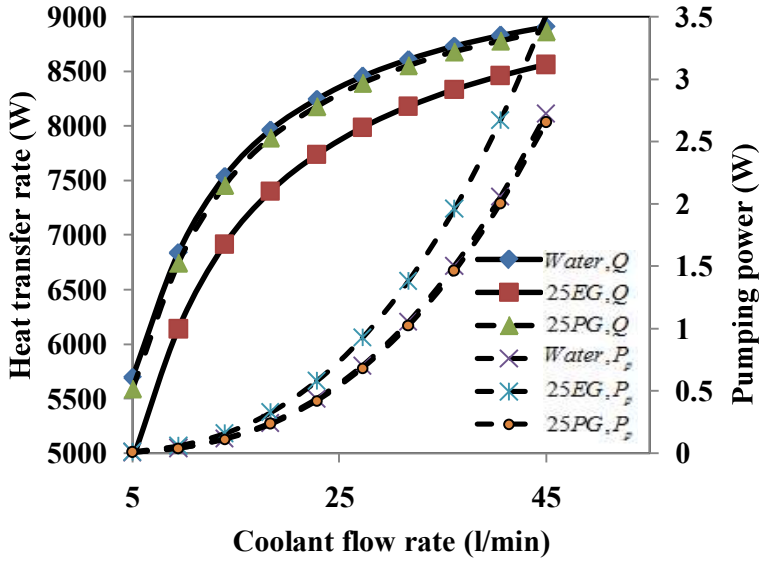

Figure 4.43: Heat transfer rate and pumping power with CFR

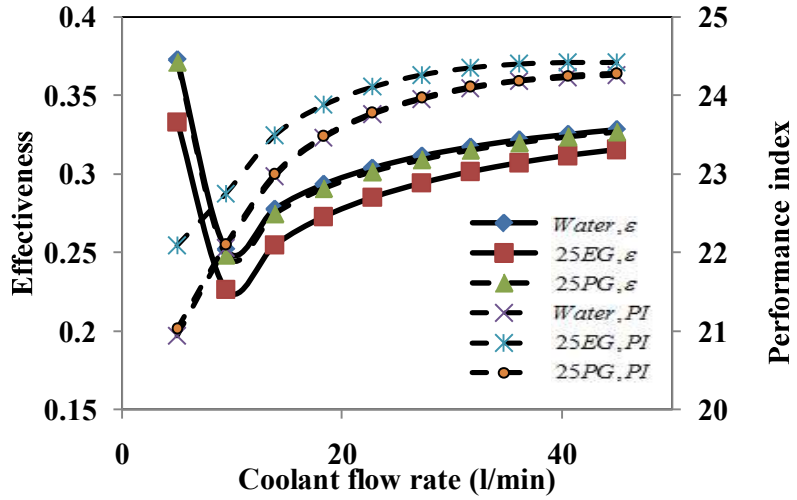

Figure 4.44: Effectiveness and performance index with CFR

However, air exit temperature is lower for 25% EG brine as compared to air exit temperature for water and optimum PG brine. Effectiveness is 50% higher for water and optimum PG brine as compared to 25% ethylene glycol brine. As shown, the effectiveness first decreases and then increases with coolant flow rate, and yields some minimum value at about 10 l/min, which is a balance condition of a heat exchanger for equal heat capacity rates of both coolant and air. Due to the

same reason, the entropy change of coolant yields minimum value for the balance condition. Performance index also gradually increases with coolant flow rate and are similar for both water and optimum PG brine.

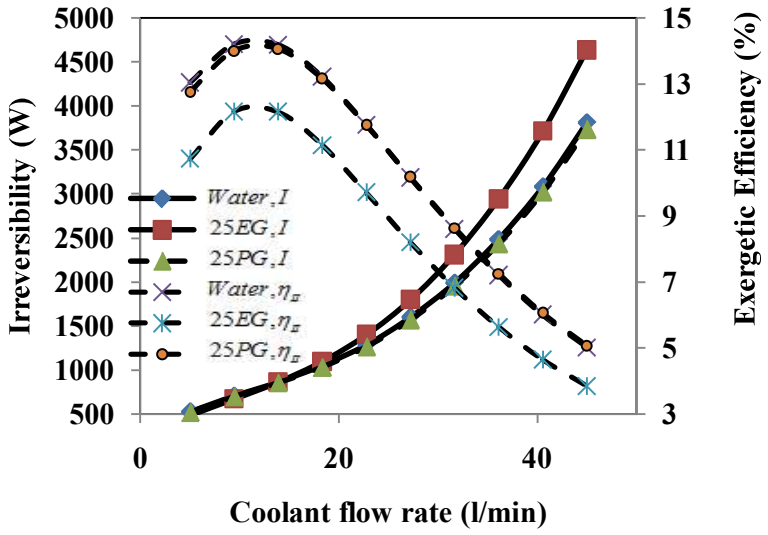

Figure 4.45: Irreversibility and exergetic efficiency with CFR

Variations of exergy changes, irreversibility and second law efficiency with coolant flow rate are shown in Figs. 4.45. Second law efficiency is 60% higher for both water and optimum PG brine as compared to 25% ethylene glycol brine and gradually decreases with increase in coolant flow rate after 10 l/min. Irreversibility monotonically increases with coolant flow rate. However, the second law efficiency is maximum at coolant flow rate of 10 l/min through the radiator due to minimum overall temperature difference between coolant and air for the balance heat exchange condition as the heat capacity ratio is unity.

The effects of air velocity on various energetic and exergetic performance parameters are shown in Figs. 4.46- 4.47 for water, 25% EG brine and 25% PG brine. Effectiveness for both water and optimum (25%) PG brine is nearly same

and gradually decreases with increases in air velocity due to the factor of efficiency of fan and fan power gradually increases with air velocity. But the irreversibility of 25% EG brine has 28.5% lower with comparison to optimum brine of PG and water.

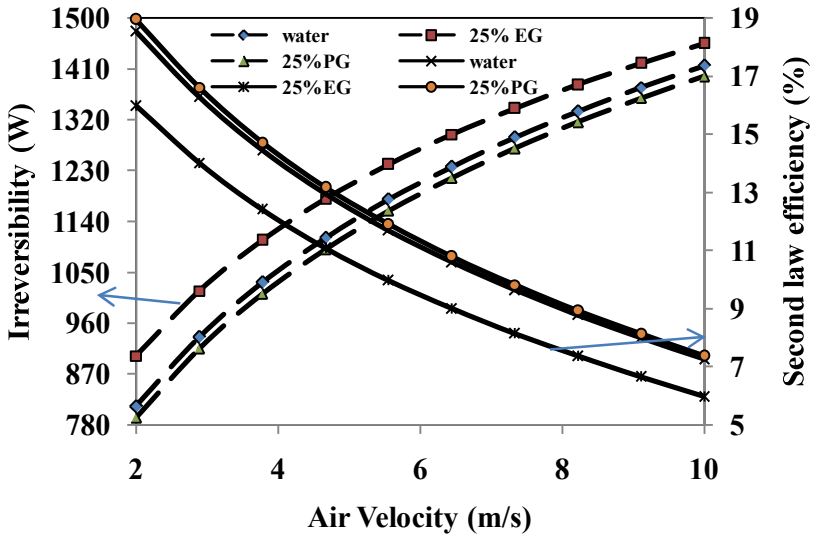

Figure 4.46: Variations of irreversibility and Second law efficiency with air velocity

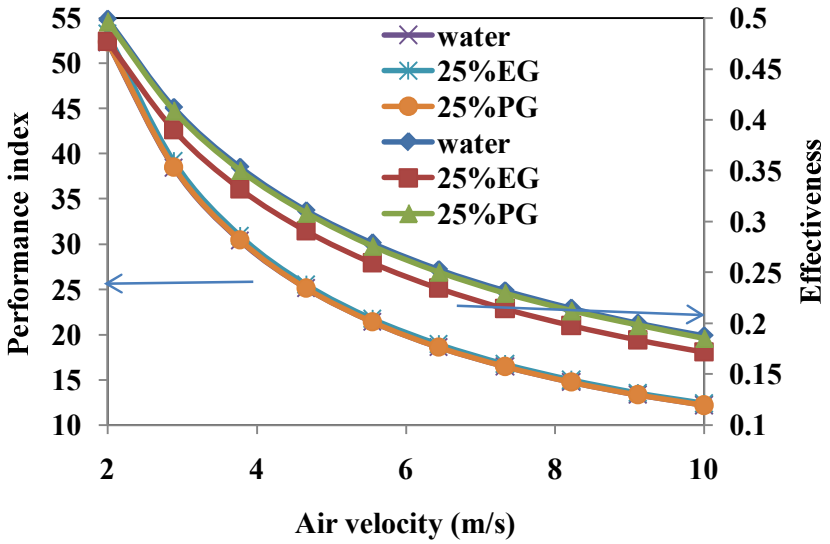

Figure 4.47: Variations of performance index and effectiveness with CFR

This is due to the higher heat transfer yields lower temperature difference between air and coolant. Second law efficiency and exergy change for air are 28.5 % higher, gradually decreases with air velocity and also nearly same for both optimum PG brine and water, as compared to 25% ethylene glycol. The present results and discussion reveal that the 25% PG brine can give similar performance as water with wider operating temperature

(b) With various coolants

Perormance analysis for heat transfer rate, effectiveness and pumping power of rectangular fin radiator are shown in Figs.4.48-4.50. Results shows that PG brine based hybrid nanofluid having higher heat transfer rate and effectiveness for a rectangular fin radiator with hydraulic diameter of 0.002m with coolant flow rate of 9 l/min. PG brine based hybrid nanofluid having higher heat tranfer coefficient and effective tharmal conductivity which results the high heat tarnsfer rate.Water and 25% PG brine results nearly same performance. However sugarcane juice as radiator coolant performs lower pumping power as compared to all mentioned coolants.

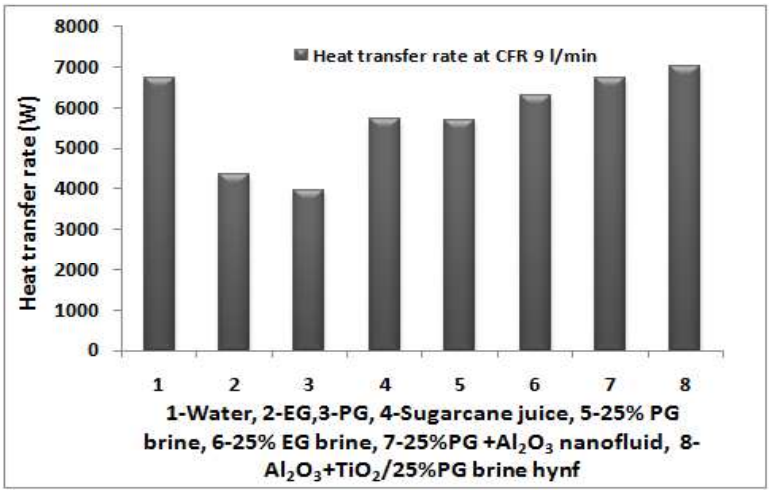

Figure 4.48: Heat transfer rate for various coolants

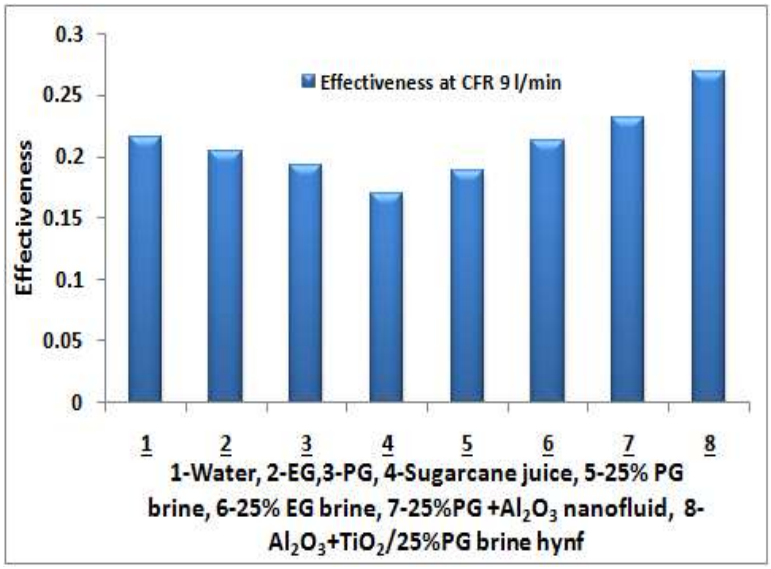

Figure 4.49: Effectiveness for various coolants

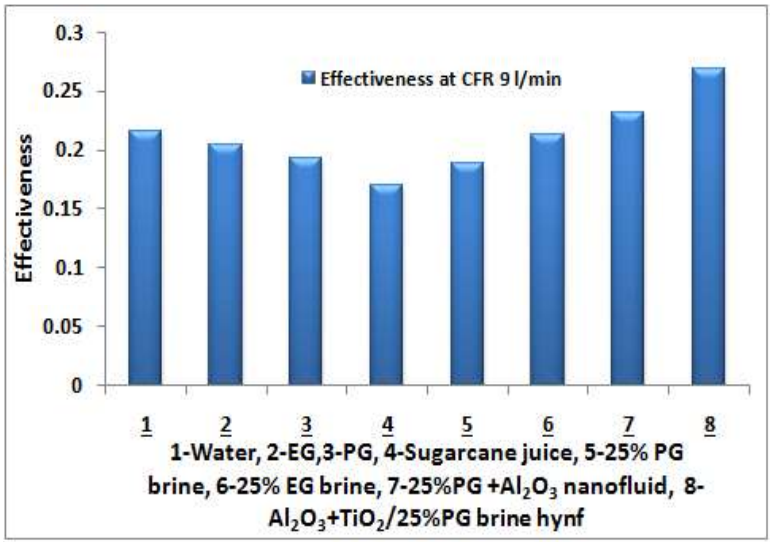

Figure 4.50: Pumping power for various coolants

4.2 Performance of radiator with different fin material

An efficient cooling system is required not only to dissipate the heat from vehicles, but also to reduce the weight of the vehicle, which will lead to less fuel consumption. In order to develop a new compact heat exchanger, a porous medium might be a good choice as material for the heat exchangers.The porous medium - graphite foam and carbon foam which was developed by Oak Ridge National Laboratory [121], has extremely high thermal conductivity. The characteristics of graphite foams and carbon foams are as follows:

(i) High thermal conductivity: The effective thermal conductivity of graphite foam with air (40-150 W/m.K) is much higher than the effective thermal conductivity of an aluminum foam (2-26 W/m.K) [6].(ii) Low density: The density of graphite foam is from 0.2 to 0.6 g/cm^3 which is about 20 % that of aluminum.(iii)Large specific surface area: Because of the open cells and inter-connected void structure, the specific surface area of graphite foam is between 5000 and 50000 m^2/m^3.(iv)Weak mechanical properties: The tensile strength of graphite foam is much lower than that of the metal foam.

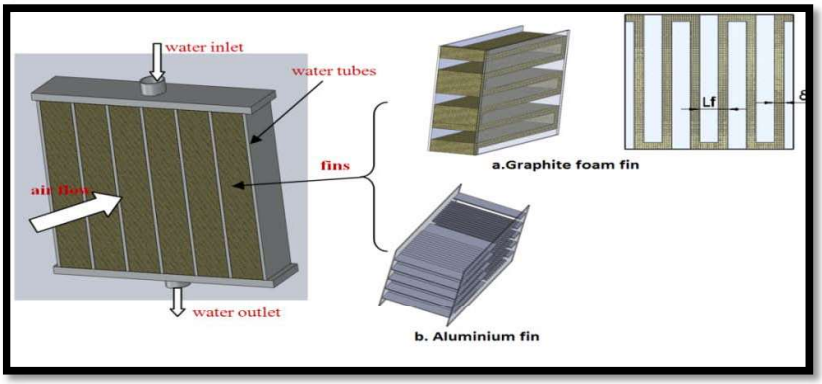

Figure 4.51: Porous media heat exchangers for radiators[6]

Based on these characteristics, the graphite foam is a potential material for heat exchangers. Application of porous media heat exchangers are shown in Fig. 4.51.

4.2.1 Mathemetical Modelling and simulation

Same assumptions have been considered as per 4.1.1 and for the evaluation of radiator performance eqs.(4.27-4.44) have been considered. Parameters of the graphite / carbon foam are: Porosity (ε) is 0.82; effective thermal conductivity (k_{eff}) is 120 W/(m.K); permeability (α) is 6.13 x 10^{-10} m^2; and the

Forchheimer coefficient C_F is 0.4457.and it depends on the porosity of the porous media.

The effective specific heat of the graphite foam,

$$c_{p,eff} = \varepsilon c_{p,f} + (1-\varepsilon) c_{p,s} \qquad (4.45)$$

Heat transfer coefficient,

$$h_a = \frac{j_a G_a C_{p,eff}}{Pr^{2/3}} \quad \text{Where,} \quad j_a = \frac{0.174}{Re_a^{0.383}} \qquad (4.46)$$

However, pressure drop in porous media using Forchheimer-extended Darcy model [6], can be calculated as

$$\frac{\Delta P}{dl} = \frac{\mu * U}{\alpha} * \frac{C * \rho * U^2}{\sqrt{\alpha}} \qquad (4.47)$$

4.2.2 Result validation

The predicted COP value of graphite foam has been compared with experimental value [6] at the same inlet conditions (*CFR = 10 l/min , T_{ai}= 30^oC T_{ci}= 80^oC*) as shown in Fig.4.52 and it is found that with increasing air velocity, the COP of graphite foam fin decreases. However, due to the high pressure drop through the graphite foam, large input pumping power is required. This causes the COP of the corrugated foam to be lower. The deviation of predicted theoretical and experimental results found to be within 4 % to 5%.

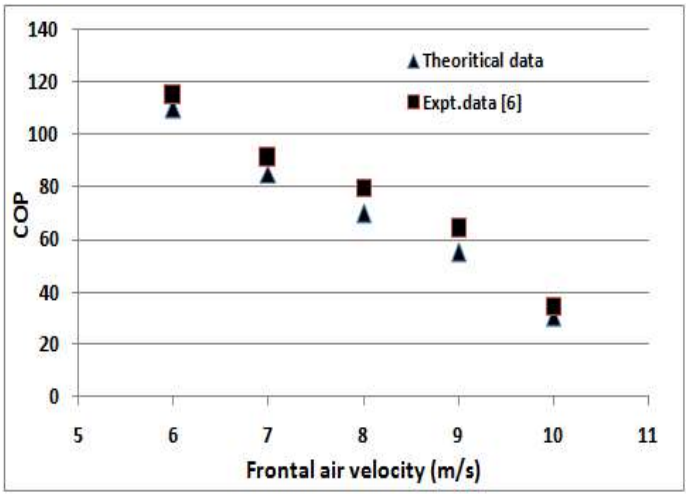

Figure 4.52 : Validation of graphite foam fin radiator

4.2.3 Results and discussions for radiator performance

Variations on heat transfer rate, air exit temperature, coolant exit temperature of various fin material with air velocity have been shown in Fig. 4.53-4.55. Results show that carbon foam and graphite foam fin radiator have higher heat transfer rate as compared to copper, aluminium and aluminium foam fin materials and increases with increase in frontal velocity due to higher thermal conductivity. Also, lower pumping power is required for aluminium and copper radiator as compared to graphite foam and carbon foam radiator. Air exit temperature is higher for carbon foam and is followed by aluminium, graphite foam, copper and aluminium foam. However, coolant exit temperature of mentioned fin materials foam gradually decreases with increase in air frontal velocity.

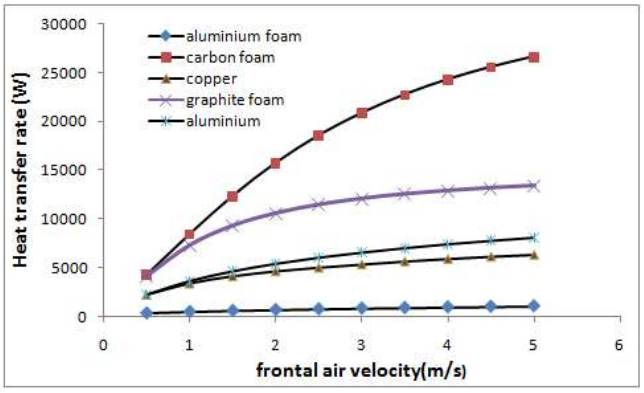

Figure 4.53: Heat transfer rate with air velocity

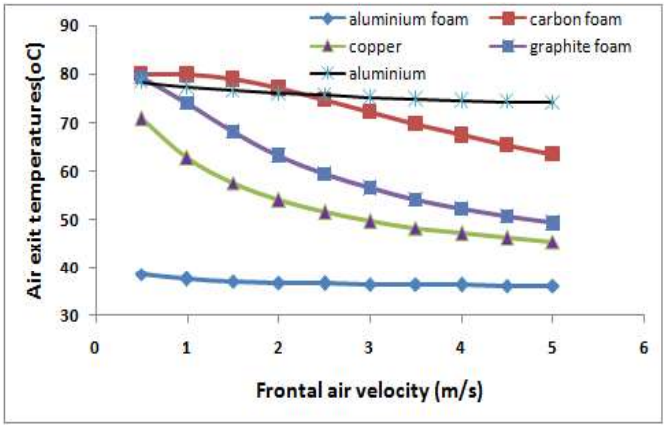

Figure 4.54 : Air exit temperature with air velocity

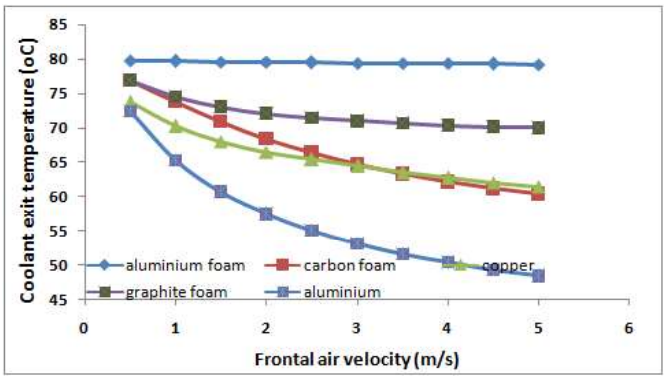

Figure 4.55: Coolant exit temperature with air velocity

Similarly with increase in frontal air velocity carbon and graphite foam fin radiator have higher pressure drop and gradually decreases with increases in frontal air velocity shown in Fig.4.56

.

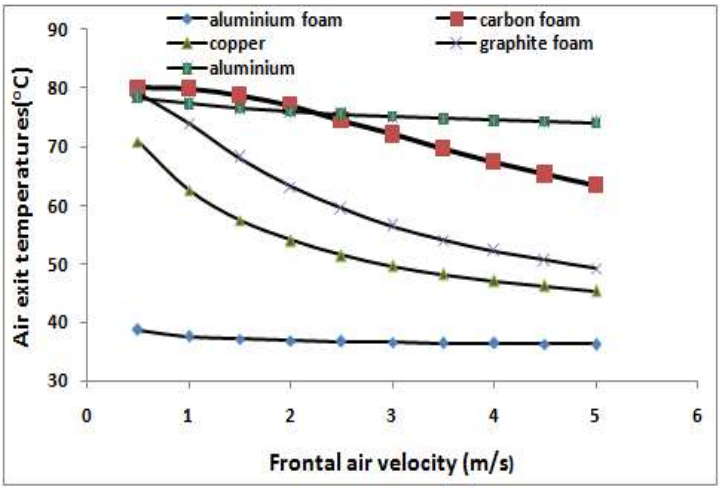

Figure 4.56: Airside pressure drop with air velocity

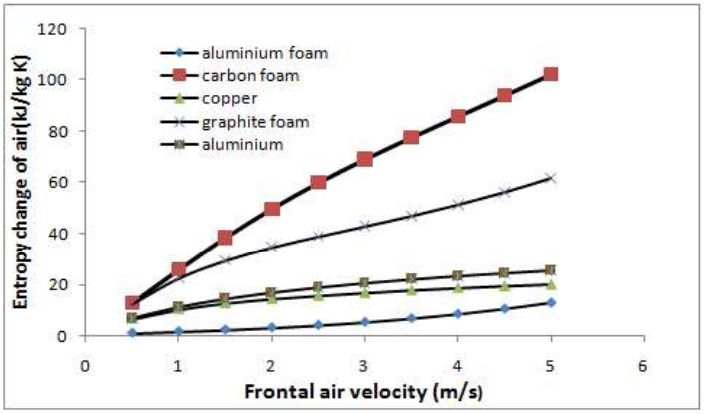

Figure 4.57: Entropy change with air velocity

Entropy change for air is higher for carbon foam as exit temperature of carbon foam is higher and followed by graphite foam, copper, aluminium and aluminium foam. Also, it gradually decrease with increases in air velocity. Thus, carbon foam results higher entropy and followed by graphite foam, copper, aluminium and aluminium foam fin as radiator materials. However, fan power for carbon foam and graphite foam gradually increases with increase in frontal velocity and followed by aluminium foam, aluminium and copper fin materials as

shown in Fig.4.58. Thus, due to the porosity of the carbon and graphite foam, it has higher pressure drop in radiator performance.

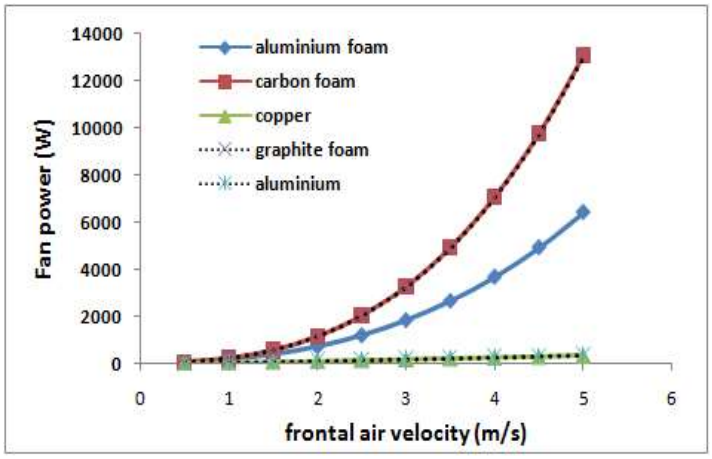

Figure 4.58: Fan power with frontal air velocity

4.3 Enhancement of cooling system using different configuration of automotive radiator

Less volume is one of the essential characteristics of a good radiator as they decrease the weight of the vehicle. So, a comparison between different radiators occupying same volume has been carried out and their cooling capacity is compared. The analysis has been made for a constant volume of $0.056m^3$, considering different arrangement of heat exchanger.

The arrangements considered include the conventional radiator having cross flow heat exchanger, a counter flow heat exchanger installed on the roof of heavy load automobiles and a combination of both these radiators called CCFC (Cross and Counter Flow Combination). Different arrangements have been compared to find out the suitable heat exchanger for heavy load automobile like trucks and buses. The configurations considered in this study are explained below-

i) Cross flow heat exchanger with both fluids unmixed, installed in the front of the automobile occupying a core volume of 0.8m*0.14m*0.5m and water as coolant.

ii) Counter flow heat exchanger installed on the roof of the automobile at an angle to the horizontal, parallel to the flow direction of air having the core volume as 0.8m*0.2m*0.35m and water as a coolant.

iii) A combination of both the above systems i.e. a cross flow heat exchanger with both fluids unmixed installed in the front of the automobile with a volume as 0.8m*0.07m*0.5m and a counter flow heat exchanger installed on the roof of the automobile at an angle parallel to the flow direction of air with a volume of 0.8m*0.1m*0.35m with water as coolant.

4.3.1 Arrangement of Radiators

All heat exchangers under consideration of this study have fins to increase the heat exchange surface area. The fins are made of aluminium (thermal conductivity 205 W/m-K at 298 K)[6]. Louver fins with a louver angle $28^o$are used in the counter flow heat exchangers along with round tubes. For the cross flow heat exchanger, plate fins having louver, with a louver angle of 16^ohave been used. Different configurations are discussed as below-

i) In first configuration, a cross flow radiator is installed in the front of the vehicle as shown in Fig.4.59. The conventional model of heat exchangers used in modern day automobiles consists of a total of 1215 water tubes [6] (81 across the length and 15 across the width) and fins offering a total heat exchange area of $897.59 m^2/m^3$. Mass flow rate of the coolant is taken as 2 kg/s.

ii) In second configuration, a counter flow heat exchanger is positioned at the roof of the truck as shown in the Fig.4.59. The radiator is installed at an angle to the horizontal, parallel to the streamline direction of flow of air at that location to maximize the air mass flow rate. Water flows from the higher side of the heat exchanger to the lower side in a direction exactly opposite to the direction of flow of air, thus giving a counter flow orientation. A total of 1326 water tubes (51 across the length and 26 layers across the height) and fins offering a total heat exchange area of 866.26m^2/m^3 have been considered for the counter flow with same core volume and mass flow rate of the coolant at 2 kg/s.

iii) The third orientation consists of both the above heat exchangers but with a volume half of the original volume of the radiators, such that the volume is not compromised but distributed. The cross flow heat exchanger and the counter flow heat exchanger in this configuration have half the width of the cross flow heat exchanger and counter flow heat exchanger used in configurations 1 and II respectively.

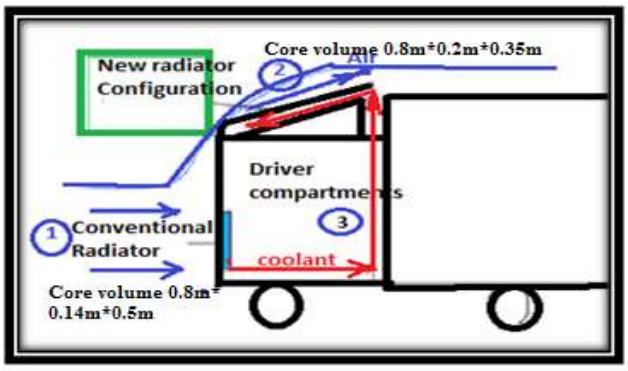

Figure 4.59: Arrangement of cross flow and counter flow configurations [6]

Initially coolant is passed through the cross flow heat exchanger and then is raised to the roof where it passes through the counter flow heat

exchanger at 2kg/s as shown in Fig.4.59. All dimensions of tube, fins and the core volume of above mentioned three configurations have been shown in Table- 4.7.

4.3.2 Mathematical modelling and simulation

Some important assumptions have been considered for configuration III radiators are given below-

(a) The temperature of coolant at the inlet of counter flow heat exchanger is same as the temperature of coolant at the exit of cross flow heat exchanger, neglecting the change in temperature due to friction losses in the connecting pipes.

(b) The temperature of air at inlet is same for both cross flow heat exchanger and counter flow heat exchanger. However, the velocity of air at the inlet of counter flow heat exchanger is different from that at the inlet of cross flow heat exchanger and it highly depends on the design of the vehicle and on the contour on which the vehicle is moving on. The pressure of air at the top of the roof is generally less than that near the bumper by 100-200 Pa [88].

(c) The velocity of air at the roof is greater than that of near the bumper and for this reason, the velocity of air at input of counter flow heat exchangers is assumed as half times of the velocity of air at the inlet of cross flow heat exchanger.

(d) For the evaluation of radiator performance eqs.(4.26-4.33) have been considered for cross flow configuration and the dimension of the three configurations have been shown in Table 4.7.

Table – 4.7 Dimensions of tubes, fins and radiators for various configurations

Configuration I (Cross flow Radiator)				**Configuration II (Counter Flow Radiator)**			
Coolant used– Water (flat tubes) *Total No. Of water tubes* = 1215 (81 across length * 15 layers across width, single pass, both fluids unmixed) *Fin type*= louver (l_a=16^0, f_p=0.00224m, l_p=0.0012m, f_h=0.01m, l_h=0.008m, l_d=0.14m)				*Coolant used*- water (round tubes) *Total No. Of Tubes* = 1326 (51 across length * 26 layers across height) *Fin type* = louver (l_a=28^0, f_p=0.00232m, l_p=0.0012m, f_h=0.016m, l_h=0.013m, l_d=0.20m)			
Sl. No.	**Description**	**Air Side**	**Coolant Side**	**Sl. No.**	**Description**	**Air Side**	**Coolant Side**
1	Fin Pitch	4.46 fins/cm		1	Fin Pitch	4.32 fins/cm	
2	Fin Thickness	0.1mm		2	Fin Thickness	0.1mm	
3	Hydraulic Diameter	0.003663 m	0.004226 m	3	Hydraulic Diameter	0.004044 m	0.003114m
4	Free Flow Area/Frontal Area	0.786	0.8	4	Free Flow Area/Frontal Area	0.8094	0.8
5	Heat Transfer Area / Total Volume	1030.288 m^2/m^3	132.7 m^2/m^3	5	Heat Transfer Area / Total Volume	938.93 m^2/m^3	72.67 m^2/m^3
6	Fin Area/ Total Area	0.8712		6	Fin Area/ Total Area	0.9237	
7	Fluid inlet temperature	30^0 C	90^0 C	7	Fluid inlet temperature	30^0 C	90^0 C
8	Core dimensions	0.8m*0.14m*0.5m		8	Core dimensions	0.8m*0.2m*0.35m	

Configuration III (CCFC Radiator)							
Cross Flow Heat Exchanger				**Counter Flow Heat Exchanger**			
Coolant used– Water (flat tubes) *Total No. Of Tubes* = 648 (81 across length * 8 layers across width, single pass, both fluids unmixed) *Fin type* = louver (l_a=16^0, f_p=0.00224m, l_p=0.0012m, f_h=0.01m, l_h=0.008m, l_d=0.07m)				*Coolant used*- water (round tubes) *Total No. Of Tubes* = 1326 (51 across length * 26 layers across height) *Fin type* = louver (l_a=28^0, f_p=0.00232m, l_p=0.0012m, f_h=0.016m, l_h=0.013m, l_d=0.10m)			
Sl. No	**Description**	**Air Side**	**Coolant Side**	**Sl. No**	**Description**	**Air Side**	**Coolant Side**

.				.			
1	Fin Pitch	4.46 fins/cm		1	Fin Pitch	4.32 fins/cm	
2	Fin Thickness	0.1mm		2	Fin Thickness	0.1mm	
3	Hydraulic Diameter	0.003663 m	0.004226 m	3	Hydraulic Diameter	0.004044 m	0.003114 m
4	Free Flow Area/Frontal Area	0.786	0.8	4	Free Flow Area/Frontal Area	0.8094	0.8
5	Heat Transfer Area / Total Volume	1030.288 m^2/m^3	132.7 m^2/m^3	5	Heat Transfer Area / Total Volume	938.93 m^2/m^3	72.67 m^2/m^3
6	Fin Area/ Total Area	0.8712		6	Fin Area/ Total Area	0.9237	
7	Fluid inlet temperature	30^0 C	90^0 C	7	Fluid inlet temperature	30^0 C	Variable
8	Core Dimensions	0.8m*0.07m*0.5m		8	Core dimensions	0.8m*0.1m* 0.35m	

The Colburn factor for louver fin configuration and the Prandtl number of air side are

$$j_a = \frac{0.26712}{Re_a{}^{0.1944}}\left(\frac{L_a}{90}\right)^{0.257}\left(\frac{F_P}{L_p}\right)^{-0.5177}\left(\frac{F_h}{L_p}\right)^{-1.9045}\left(\frac{L_h}{L_p}\right)^{1.7159}\left(\frac{L_d}{L_p}\right)^{-0.2147}\left(\frac{t}{L_p}\right)^{-0.05} \quad (4.48)$$

$$Pr_a = \frac{C_{p,a}\mu_a}{k_a} \quad (4.49)$$

With Colburn factor the heat transfer coefficient of air is

$$h_a = \frac{j_a G_a C_{p,a}}{Pr_a^{2/3}} \quad (4.50)$$

Nusselt number for the coolant,

$$Nu_f = 0.023 Re_f^{0.8} Pr_f^{0.3} \quad (4.51)$$

Heat transfer coefficient of fluid ,

$$h_f = \frac{Nu_f k_f}{D_{h,f}} \quad (4.52)$$

For a counter flow heat exchanger, the effectiveness [5],

$$\varepsilon = \frac{1-\exp\left(-NTU\,(1-C^*)\right)}{1-C^*\exp\left(-NTU\,(1-C^*)\right)} \qquad (4.53)$$

4.3.3 Results and discussions

4.3.3.1 Optimization of the counter flow volume

In configurations II and III, the volume occupied by the counter flow heat exchanger is V and V/2 respectively. This volume needs to be distributed among length, breadth and height of the heat exchanger so that maximum heat transfer obtained. For this, the length of the radiator kept constant, the width and height parameters are varied with maintaining a constant volume of radiator for calculation the heat transfer coefficient.

A parameter p is defined which accounts for the variation in the width and the height of the radiator as,

Length = 0.8 m

Width = (0.14 * p * k) m

Height = (0.5 / p) m (4.54)

Here k=1 for configuration II and k=0.5 for configuration III.

The variation of thermal conductance and effectiveness with radiator height have been shown in (Fig.4.60- 4.61) only for configuration II. Results show that thermal conductance increases whereas effectiveness decreases with increase in height of radiator. This is due to the reason that, conductance increases due to increase in area with variation in height of the radiator. However, NTU decreases due to increase in C_{min}(air side heat capacity rate) which leads to decrease in effectiveness with increase on height of radiator.

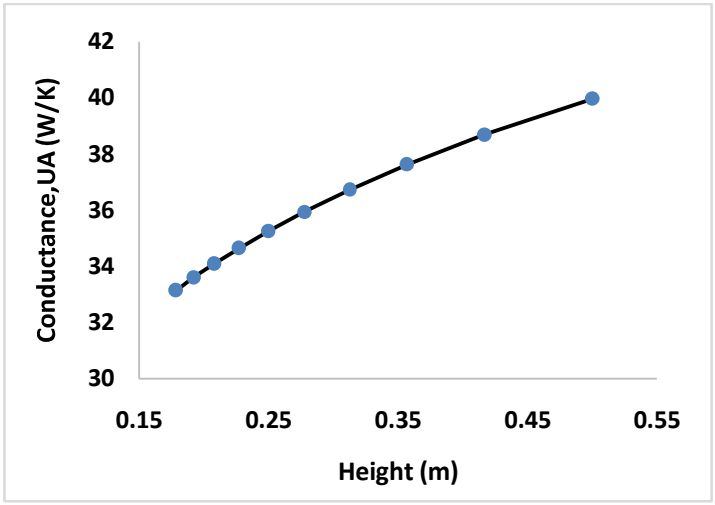

Figure 4.60: Variation of thermal conductance (Configuration-II)

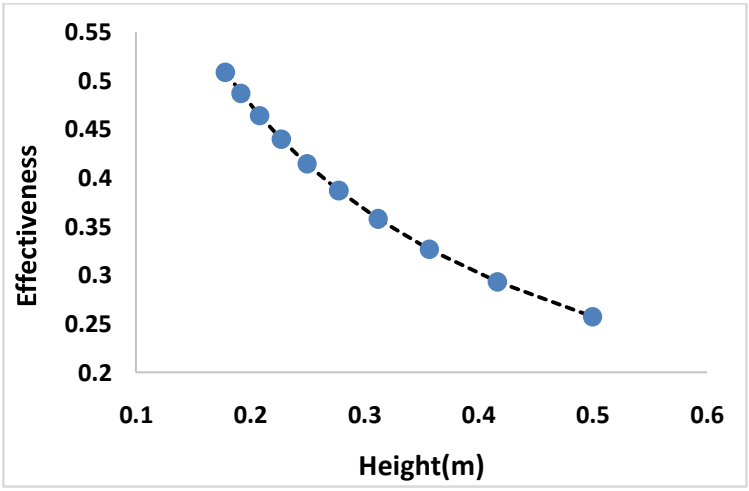

Figure 4.61 : Variation of effectiveness with height (Configuration II)

However, with increase in the height of the radiator, the frontal area of the radiator also increases due to the mass flow rate of air which leads to the significant increase in heat transfer rate as shown in Fig.4.62

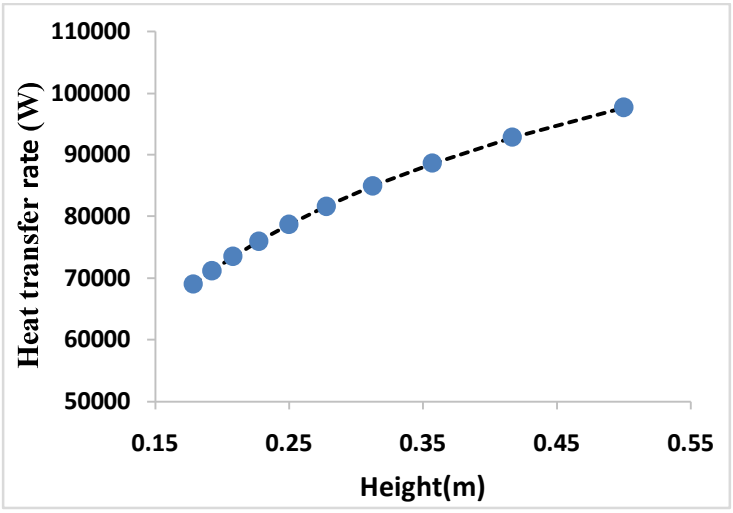

Figure 4.62: Variation of cooling capacity with height (Configuration II)

So for the maximum heat dissipation from the fluid, the height of the heat exchanger should be as high as possible. The major problem in increasing the height of counter flow radiator occurred due to its installation the roof of the automobiles. Hence, a radiator having higher height tends to disturb the usual streamline flow of air around the vehicle and starts to offer more resistance to movement of vehicle in forward direction. Hence, for purpose of optimization the height of the radiator in both configurations II and III has been considered as 0.35 m.

4.3.3.2 Optimization of angle of counter flow heat exchanger

The optimum angle at which counter flow heat exchanger is placed in a heavy load vehicle depends on the design of the automobile. It is to be noticed that for any design of the automobile, a streamline flow of air is developed when it moves at a steady speed. If the counter flow heat exchanger is placed at an angle same as the direction of the air flow, then maximum air moves into the heat exchanger. Otherwise, only a component of the air flow goes into the heat exchanger. Also, due to the change in the mass flow rate of air into the heat

exchanger, the cooling capacity of the heat exchanger changes with the angle at which the counter flow heat exchanger is placed. Describing the input velocity u' of air into the counter flow heat exchanger as

$$u' = u\cos(\theta - \theta_o) \qquad (4.55)$$

where, u is the maximum velocity of air flowing into counter flow heat exchanger. To calculate the angle for optimum performance, cooling capacity of counter flow heat exchanger in configuration II as shown in Fig.4.63, the truck considered in the study is designed in a manner, so that the streamlines near the counter flow heat exchanger were inclined at 30 degrees to the horizontal for the maximum mass flow rate of air for better cooling capacity of the radiator.

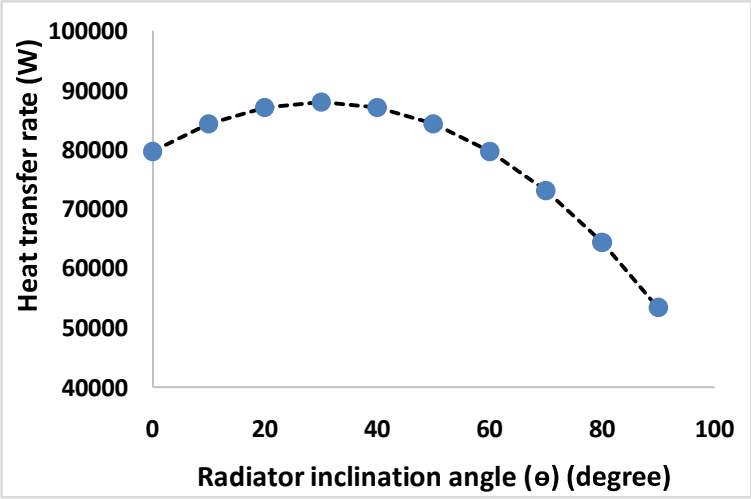

Figure 4.63: Heat transfer rate with radiator inclination (Confg.II)

4.3.3.3 Result validation

The predicted result is validated with theoretical results [6] for louvered fin counterflow configuration for the parameters heat transfer coefficient and pressure drop as shown in Fig.4.64. The deviation between the results for heat transfer coefficient and pressure drop are 4.4% and 5.2% respectively for a

coolant mass flow rate of 2 kg/sec. Thus, there is a good agreement between the predicted and theoretical results, in terms of thermal performance.

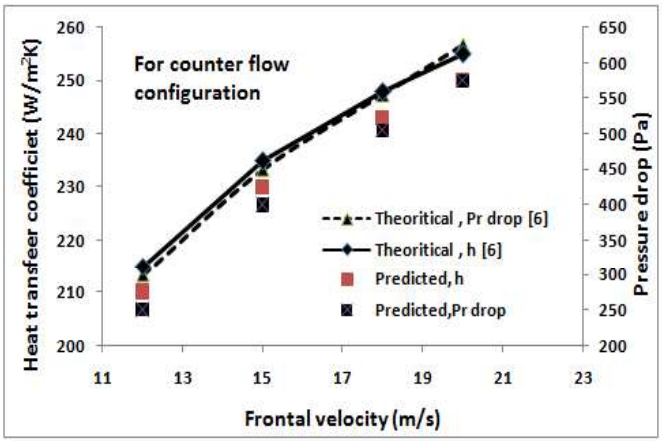

Figure 4.64: Validation results for counter flow configuration [6]

4.3.3.4 Performance comparison for various configurations

Variation of heat transfer rate with air velocity and mass flow rate of coolant have been compared as shown in Fig.4.65- 4.66, at a mass flow rate of 2 kg/s for the three configurations of radiator. A typical automobile usually runs between 20 km/hr and 80 km/hr depending upon the traffic conditions. Change in the speed of the vehicle also changes the mass flow rate of air for both counter flow and cross flow heat exchangers. Results shows that with increase in vehicle speed the heat capacity rate increases due to which the Reynolds number increases and hence the heat transfer coefficient of air increases which leads to increase the cooling capacity of the radiator.

Also, the CCFC radiator dissipate the maximum heat, for all vehicle speeds whereas the counter flow radiator dissipated the minimum. At 40 km/hr (11.11 m/s) cross flow heat exchanger dissipates 123.36 kW of heat whereas

CCFC dissipates 167.29 kW of heat, i.e an improvement of 43.93 kW of cooling capacity.

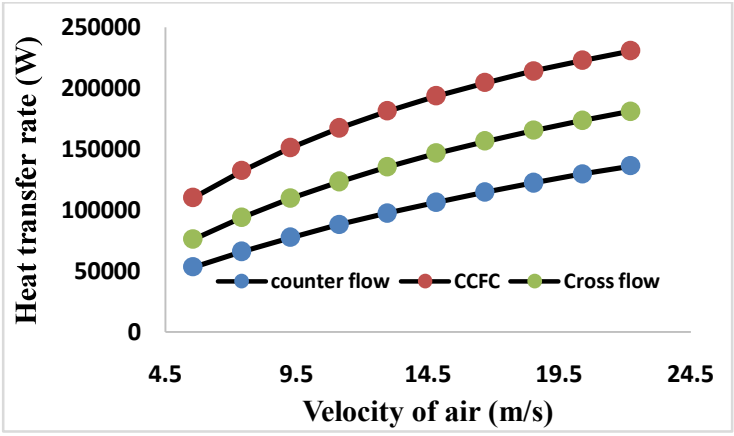

Figure 4.65: Heat transfer rate with velocity of air

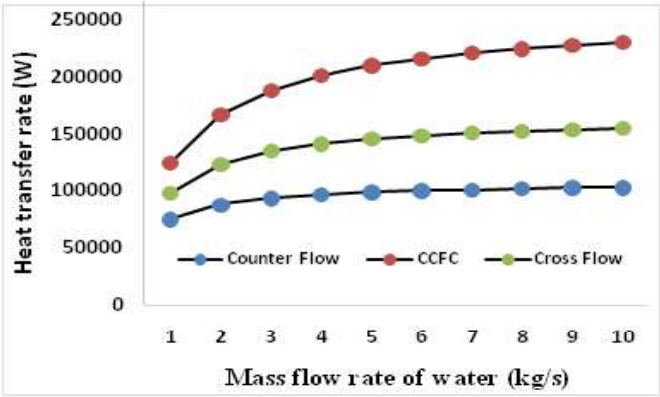

Figure 4.66: Heat transfer rate with mass flow rate of coolant

Also, increase in mass flow rate of coolant results increase in Nusselt's number which leads to increase in the heat transfer coefficient of coolant with increase in cooling capacity of radiator. Typical mass flow rate of coolants for the radiator are between 2-4 kg/s and within this range the cooling capacity of CCFC turns out to be better than cross flow radiators.

Pressure drop through pipes in a heat exchanger should be as low as possible, as it demands the power from water pump to keep the coolant flow in the radiator.

Fig. 4.67 shows that, the pumping power required for cross-counter flow combination (CCFC), is more than the other two basic configurations for mass flow rate of fluid.

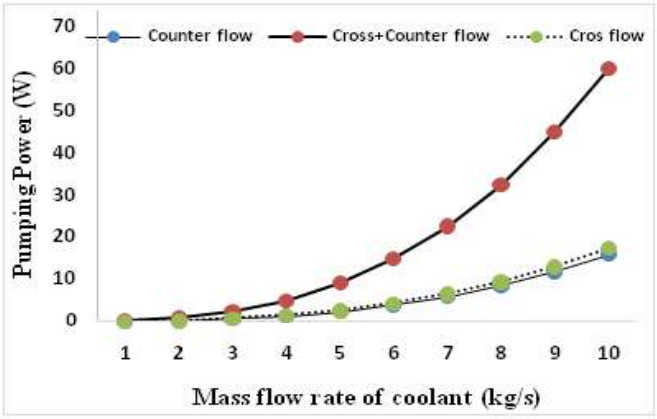

Figure 4.67: Pumping power with mass flow rate of coolant

Indeed, the difference between the required pumping power in CCFC and other two configurations, increase with increase in mass flow rate of fluid. However, with practical perspective, the amount of fluid required to be cooled for an engine is roughly 2- 4 kg/s and results shows that, the pumping power required is less than 10W which is quite less and hence higher pumping power for CCFC is not a very big disadvantage for it.

The velocity of air near the roof of vehicle is more than that at the hood (where the cross flow heat exchanger is placed).Generally the ratio between velocity of air near the roof and the velocity of air near the hood lies with a range between 1-1.5. For this, the cooling capacity of different configurations of radiators are compared at constant vehicle speed, input velocity of air at hood and mass flow rate of coolant and with the varying ratio of velocities between counter flow and cross flow heat exchangers. Results show from Fig.4.68, that the change

in ratio between the air velocity has no effect on cooling performance of cross flow radiators.

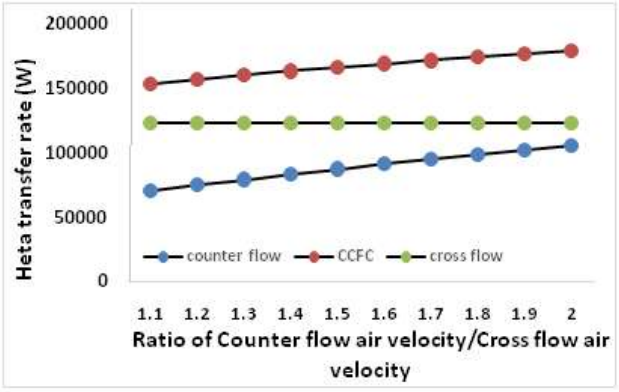

Figure 4.68: Heat transfer rate with ratio of counter /cross flow air velocity

However, the heat transfer rate for configurations II and III improve as the ratio increases. Also the CCFC radiator has the highest heat transfer rate for all the ratios and hence proves to be better than conventional cross flow radiators.

Major outcomes from theoriical analysis of prsent chapter ;

- Sugarcane juice yields better heat transfer, effectiveness, pumping power and exergetic efficiency characteristics at higher temperature (approximately above 60^{o}C) and significantly better than water, nanofluid, EG and PG.
- Among all the studied hybrid nanofluids water based Ag hybrid nanofluid has higher heat transfer coefficient, thermal conductivity ,effectiveness and heat transfer rate with comparison to 1% volume fraction Al_2O_3 nanofluid and is followed by 1% volume fraction (50/50) of Cu,CuO,Fe_2O_3,TiO_2 hybrid nanofluids.
- Brine concentration of 25% propylene glycol results highest performance index, heat transfer, effectiveness with lowest pumping power. Also it yields

nearly same performance as water at higher temperature as coolant for radiator.

- Louvered fin radiator results the better performance as compared to wavy and rectangular fin radiator.
- Heat transfer rate and effectiveness of carbon foam fin radiator is higher and increases with frontal velocity, followed by graphite foam, copper, aluminium and aluminium foam fin material for radiator.
- For the same volume occupied by the cross flow radiator and CCFC radiator, the CCFC radiator has better cooling capacity than conventional cross flow radiators.